nature cell biology

ARTICLES

https://doi.org/10.1038/s41556-020-0503-2

Check for updates

Merkel cell polyomavirus activates LSD1-mediated blockade of non-canonical BAF to regulate transformation and tumorigenesis

Donglim Esther Park[1,2], Jingwei Cheng[2,3], John P. McGrath[4], Matthew Y. Lim[1,5], Camille Cushman[1,2], Selene K. Swanson[6], Michelle L. Tillgren[7], Joao A. Paulo[5], Prafulla C. Gokhale[7], Laurence Florens[6], Michael P. Washburn[6,8], Patrick Trojer[4] and James A. DeCaprio[1,2,3]✉

Merkel cell carcinoma (MCC)—a neuroendocrine cancer of the skin—is caused by the integration of Merkel cell polyomavirus and persistent expression of large T antigen and small T antigen. We report that small T antigen in complex with MYCL and the EP400 complex activates the expression of LSD1 (KDM1A), RCOR2 and INSM1 to repress gene expression by the lineage transcription factor ATOH1. LSD1 inhibition reduces the growth of MCC in vitro and in vivo. Through a forward-genetics CRISPR–Cas9 screen, we identified an antagonistic relationship between LSD1 and the non-canonical BAF (ncBAF) chromatin remodelling complex. Changes in gene expression and chromatin accessibility caused by LSD1 inhibition were partially rescued by BRD9 inhibition, revealing that LSD1 and ncBAF antagonistically regulate an overlapping set of genes. Our work provides mechanistic insight into the dependence of MCC on LSD1 and a tumour suppressor role for ncBAF in cancer.

Approximately 80% of Merkel cell carcinoma (MCC) contains integrated Merkel cell polyomavirus (MCV) DNA and expression of viral large T antigen and small T antigen[1]. MCV large T antigen and small T antigen function as oncoproteins, maintaining the viability of virus-positive MCC cell lines, promoting cellular transformation and inducing tumour formation in mice[2]. MCC harbouring MCV typically contains few cellular mutations, consistent with a significant role for large T antigen and small T antigen in MCC oncogenesis[3]. In contrast, virus-negative MCC contains many somatic mutations due to sunlight exposure. Both types of MCC share certain histological features with normal Merkel cells, including expression of KRT20 (CK20) and chromogranin A[4].

MCV small T antigen recruits MYCL (L-Myc) and MAX to the EP400 (p400) transcriptional activator complex. This activity is required for the small T antigen-mediated transformation of normal cells[5]. To identify genes regulated by the small T antigen–MYCL–EP400 complex, chromatin immunoprecipitation sequencing (ChIP-Seq) of small T antigen, MAX and EP400 and RNA sequencing (RNA-Seq) following depletion of *EP400*, *MYCL* or small T antigen was performed in MCC cell lines[5]. One validated target gene of the small T antigen–MYCL–EP400 complex is MDM2, which represses wild-type p53 activity in virus-positive MCC[6].

Lysine-specific histone demethylase 1 (LSD1) is a histone demethylase that removes H3K4 mono- and dimethylation transcription marks[7]. An alternatively spliced form of LSD1 (+8a) can demethylate H3K9me[8]. LSD1 assembles into a core ternary transcriptional repressor complex containing RCOR1 (CoREST), RCOR2 or RCOR3 and is recruited to chromatin by the SNAG domain-containing proteins INSM1, GFI1, GFI1B, SNAI1 and SNAI2, which play key roles in development and oncogenesis[9,10].

Small-molecule inhibitors of LSD1 have promising activity in preclinical models of acute myeloid leukaemia, small cell lung cancer and medulloblastoma[11–14]. In addition to inactivating its enzymatic activity, some LSD1 inhibitors disrupt the interaction between LSD1 and SNAG domain proteins[10] and the interaction with chromatin[11]. The exact mechanism of how LSD1 inhibition interferes with cancer cell growth is yet to be determined[12].

The mammalian SWI/SNF (mSWI/SNF) and BRG1/BRM-associated factor (BAF) complexes contribute to the regulation of genes involved in differentiation[15]. Over 20% of all human cancers harbour mutations in mSWI/SNF complex components[15]. The 29 gene products assemble combinatorially to produce three related mSWI/SNF complexes: canonical BAF, polybromo-associated BAF (PBAF) and non-canonical BAF (ncBAF)[15–17]. Each complex contains SMARCA4 (BRG1) or SMARCA2 (BRM) but they are distinguished by complex-specific subunits[15,16]. BRD9—a BET family protein that reads acetylated lysine histone marks—is unique to the ncBAF complex along with GLTSCR1 (BICRA) and GLTSCR1-like (BICRAL)[16,17]. Targeting the ncBAF complex confers synthetic lethality in synovial sarcoma and malignant rhabdoid tumours, and mis-splicing of BRD9 provides growth advantages in SF3B1-mutated cancers, suggesting a specific role in cancer[16–19].

Results

MCV small T antigen activates the LSD1 repressor complex. RNA-Seq performed on MCC cell lines after RNA interference-mediated knockdown of MYCL, EP400 or small T antigen identified

[1]Program in Virology, Graduate School of Arts and Sciences, Harvard University, Cambridge, MA, USA. [2]Department of Medical Oncology, Dana-Farber Cancer Institute, Boston, MA, USA. [3]Department of Medicine, Brigham and Women's Hospital, Harvard Medical School, Boston, MA, USA. [4]Constellation Pharmaceuticals, Cambridge, MA, USA. [5]Department of Cell Biology, Harvard Medical School, Boston, MA, USA. [6]Stowers Institute for Medical Research, Kansas City, MO, USA. [7]Experimental Therapeutics Core, Belfer Center for Applied Cancer Science, Dana-Farber Cancer Institute, Boston, MA, USA. [8]Department of Pathology and Laboratory Medicine, University of Kansas Medical Center, Kansas City, KS, USA.
✉e-mail: james_decaprio@dfci.harvard.edu

changes in the levels of many expressed genes[5]. Integrative analysis of RNA-Seq and ChIP-Seq revealed that reduced levels of genes were significantly associated with promoters bound by small T antigen, MAX and EP400 (Extended Data Fig. 1a). In contrast with genes directly activated by the small T antigen–MYCL–EP400 complex, depletion of EP400, MYCL or small T antigen led to increased levels of genes in differentiation and cancer pathways (Extended Data Fig. 1d and Supplementary Tables 1–3). We suspected that MCV small T antigen could transactivate a transcriptional repressor and identified several components of a histone demethylase complex, including LSD1 (KDM1A), RCOR2 and INSM1 (Fig. 1a–c and Extended Data Fig. 1b,e). Depletion of EP400 led to reduced levels of *RCOR2* and *LSD1* messenger RNA (mRNA), as determined by quantitative reverse-transcription PCR (RT-qPCR) (Fig. 1d and Extended Data Fig. 1c). While LSD1 expression is ubiquitous, RCOR2 expression is developmentally stage specific and INSM1 is predominantly expressed in developing neuroendocrine tissues and the nervous system[20]. INSM1 has been reported to be a specific immunohistochemical marker for MCC[21].

We performed large-scale immunoprecipitation with antibodies specific for endogenous RCOR2 and LSD1 in megakaryoblastic leukaemia 1 (MKL-1) and WaGa MCC cell lines, followed by multidimensional protein identification technology (MudPIT), to identify associated proteins[22]. LSD1 and RCOR2 formed a complex with INSM1 in MCC cells, together with HDAC1 and other reported components of the CoREST complex (Fig. 1f and Supplementary Table 4)[23]. Chromatin immunoprecipitation quantitative PCR (ChIP-qPCR) confirmed specific binding of small T antigen, MAX and EP400 to promoters of RCOR2 and LSD1 (Fig. 1e).

We previously reported that MCV T antigens could induce anchorage-independent growth of IMR90 fibroblasts that co-expressed a dominant-negative form of p53 (p53DD), hTERT and MYCL (L) called PHL cells[5,24]. To determine whether the expression of MCV T antigens affected levels of LSD1, RCOR2 and INSM1, RNA and protein levels were assessed in PHL cells with or without MCV T antigens (Fig. 1g,h). T antigens increased the levels of LSD1 and RCOR2 but not INSM1. Furthermore, LSD1 could specifically co-immunoprecipitate RCOR2 in PHL cells with MCV T antigens (Fig. 1i). ChIP-qPCR for small T antigen, MAX and EP400 was performed to assess enrichment for the promoters of LSD1 and RCOR2 (Fig. 1j). We found that MAX and EP400 enrichment increased in the presence of T antigens. These results indicate that small T antigen–MYCL–EP400 can activate expression of the LSD1 complex components. Of note, expression of a small T antigen mutant unable to bind the EP400 complex in PHL cells (PH2L) increased the levels of LSD1 and RCOR2, suggesting that T antigens may have additional means to activate these genes (Extended Data Fig. 1f,g).

LSD1 inhibition abrogates T antigen-driven transformation. We assessed RNA and protein levels of RCOR2, LSD1 and INSM1 in several virus-positive (MKL-1, MKL-2, MS-1, WaGa, PeTa and BroLi) and virus-negative MCC cell lines (UISO, MCC13 and MCC26) and human foreskin fibroblasts (HFFs). LSD1, RCOR2 and INSM1 transcripts (Fig. 2a–c) and protein (Fig. 2d) were significantly more abundant in the virus-positive MCC cell lines than in virus-negative MCC cell lines or HFFs. Although there is controversy regarding the ontology of the virus-negative MCC cell lines, the results showed that MCC cell lines expressing T antigens expressed LSD1, RCOR2 and INSM1 abundantly.

To determine whether MCC cell lines were sensitive to LSD1 inhibition, we treated the same panel of MCC cell lines with the LSD1 inhibitors GSK2879552, CPI-242 and GSK-LSD1 (ref. [12]). Cell viability was assessed by CellTiter-Glo assay after 12 d of treatment (Fig. 2e,f and Extended Data Fig. 2). All virus-positive MCC cell lines tested were sensitive to nanomolar concentrations of LSD1 inhibitors, whereas the virus-negative cell lines were highly resistant.

To determine whether the transformation of normal cells by MCV T antigens required LSD1 activity, we performed an anchorage-independent growth assay using MKL-1 and PHL cells with MCV T antigens[24] (Fig. 2g,h). Addition of the GSK-LSD1 inhibitor reduced the transformed phenotype of PHL cells with MCV T antigens, as shown by the reduced number of colonies formed when cultured in soft agar. Similarly, virus-positive MKL-1 MCC cells were able to grow in soft agar, but treatment with the GSK-LSD1 inhibitor completely blocked colony formation.

Integrated LSD1 target analysis reveals critical gene expression changes during LSD1 inhibition. The virus-positive MCC cells grew as loose clusters in suspension and formed tight floating spheroids in the presence of LSD1 inhibitors (Fig. 2i). To assess for changes in gene expression, RNA-Seq was performed on six virus-positive cell lines and the virus-negative UISO MCC cell line treated with various LSD1 inhibitors for 1 or 3 d (Fig. 3a–c). Despite differences in the treatment parameters, similar gene expression changes were observed in response to LSD1 inhibition in all six virus-positive cell lines but not in the UISO cells when assessed by RNA-Seq and RT-qPCR (Fig. 3b,d). Principal component analysis (PCA) of the RNA-Seq data showed similar global shift changes in gene expression in all six virus-positive MCC cell lines with LSD1 inhibition (Fig. 3c). The levels of many genes, including *FAM5B* (*BRINP2*), *ID1*, *CDH11*, *CALB2*, *PROM1*, *GFI1*, *SMARCA1*, *SMAD9*, *ID2* and *HES1*, were significantly increased by LSD1 inhibition in virus-positive cells but not in virus-negative cells (Fig. 3a,b,d and Extended Data Fig. 3a,b,d). These changes were accompanied by increased levels of H3K4me1 but not H3K4me2, suggesting that LSD1 inhibition specifically targets mono-methylation of H3K4 in MCC cells (Fig. 3e).

The LSD1 target gene analysis predicted that bone morphogenetic protein (BMP) signalling factors, including inhibitors of DNA binding 1 (ID1), ID2, ID3 and SMAD9 were targets (Fig. 3 and Extended Data Fig. 3b–d). The BMP pathway regulates embryonic patterning and neuroectodermal development[25]. Soluble BMP proteins bind to their receptors to promote phosphorylation of SMAD1, SMAD5 and SMAD9, which, in turn, transactivates specific target genes, including inhibitors of DNA binding[25]. To determine whether LSD1 inhibition activates BMP, we performed western blotting and observed increased phosphorylation of SMAD1, SMAD5 and SMAD9, as well as increased levels of ID1 RNA and protein (Fig. 3e–h and Extended Data Fig. 3c).

To test the specificity of the LSD1 inhibitors, we depleted LSD1 using a short hairpin RNA (shRNA) in MKL-1 and WaGa cells and assessed the levels of LSD1 target genes by western blotting (Fig. 3g). We found that knockdown of LSD1 led to increased levels of PROM1, ID1 and SMARCA1, similar to their response to LSD1 inhibitors. LSD1 inhibitor did not affect the protein levels of ID1, PROM1 and SMARCA1 in the virus-negative MCC cell lines (Fig. 3h).

To identify genes directly regulated by the LSD1 repressor complex, we performed ChIP-Seq of LSD1 and RCOR2 in MKL-1 cells (Fig. 4a and Extended Data Fig. 4). We observed that LSD1 and RCOR2 peaks were enriched in the genes whose expression was perturbed by LSD1 inhibition, such as *SMAD9*, *HES1* and *ID1* (Fig. 4b). RNA-Seq was correlated with LSD1 ChIP-Seq[26] to identify LSD1 targets (1,567 genes) in MCC cell lines (Supplementary Table 5). Remarkably, target genes directly repressed by LSD1 in MCC were enriched in similar pathways to those in which genes were upregulated by EP400 depletion (Extended Data Figs. 1d and 3e,f and Supplementary Tables 6, 7 and 9). These pathways included neuron development, as well as BMP and transcription growth factor-β signalling.

To gain insight into the gene expression program regulated by LSD1 in MCC, we performed motif identification analysis of

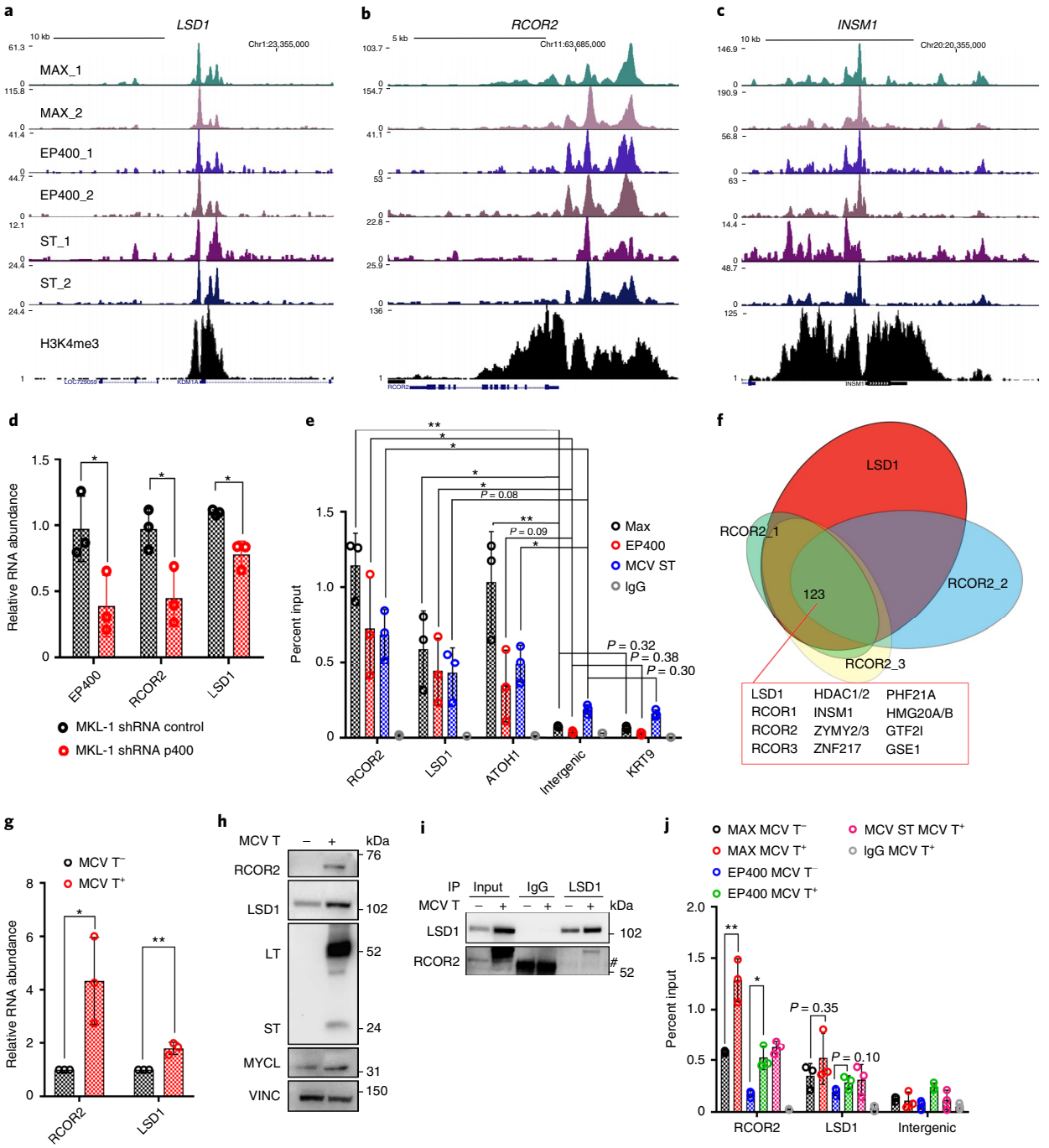

Fig. 1 | MCV small T antigen transactivates components of the LSD1 complex. a–c, Two biological replicates each of MAX (MAX_1 and MAX_2), EP400 (EP400_1 and EP400_2) and MCV small T antigen (ST_1 and ST_2) ChIP-Seq revealed that MCV small T antigen in a complex with MAX and EP400 binds to the promoters of *LSD1* (KDM1A) (**a**), *RCOR2* (**b**) and *INSM1* (**c**). The University of California Santa Cruz Genome Browser was used to visualize the peaks[41]. **d**, RT-qPCR assessment of EP400, RCOR2 and LSD1 levels after the expression of inducible EP400 or control shRNA in MKL-1 cells. The data are presented as the means of $n = 3$ biologically independent samples ± s.d. (two-sided *t*-test). **e**, ChIP-qPCR indicating that MAX, EP400 and MCV small T antigen (ST) bind specifically to RCOR2, LSD1 and ATOH1 promoters in MKL-1 cells. The KRT9 promoter and intergenic region served as negative controls. The data are presented as the means of $n = 3$ biologically independent samples ± s.d. (two-sided *t*-test). **f**, Immunoprecipitation and mass spectrometry analysis (MudPIT) showing that LSD1 and RCOR2 form a multi-protein complex in MCC cell lines. The Venn diagram shows 123 overlapping binding partners of LSD1 and RCOR2 from four independent mass spectrometry analyses. **g**, PHL cells with MCV T antigens (MCV T$^+$) have increased levels of *RCOR2* and *LSD1* mRNA. The INSM1 levels were below detection limits in PHL cells. The signals were normalized to RPLP0. The data are presented as the means of $n = 3$ biologically independent samples ± s.d. (two-sided *t*-test). **h**, PHL cells with MCV T antigens had increased protein levels of RCOR2 and LSD1. Experiments were performed at least three times. **i**, RCOR2 levels increase, and LSD1 binds to RCOR2, in PHL cells transformed with MCV T antigens. Immunoprecipitation (IP) of LSD1, followed by western blotting, was performed three times. The hashtag represents a non-specific band. **j**, ChIP-qPCR of MAX, EP400 and MCV small T antigen in PHL cells expressing T antigens indicated that T antigens enhance MAX and EP400 binding to the RCOR2 promoter. The data are presented as the means of $n = 3$ biologically independent samples ± s.d. (two-sided *t*-test). $^*P < 0.05$; $^{**}P < 0.005$. IgG, immunoglobulin G; LT, MCV large T antigen; VINC, vinculin. Unprocessed western blots are available as source data for **h** and **i**.

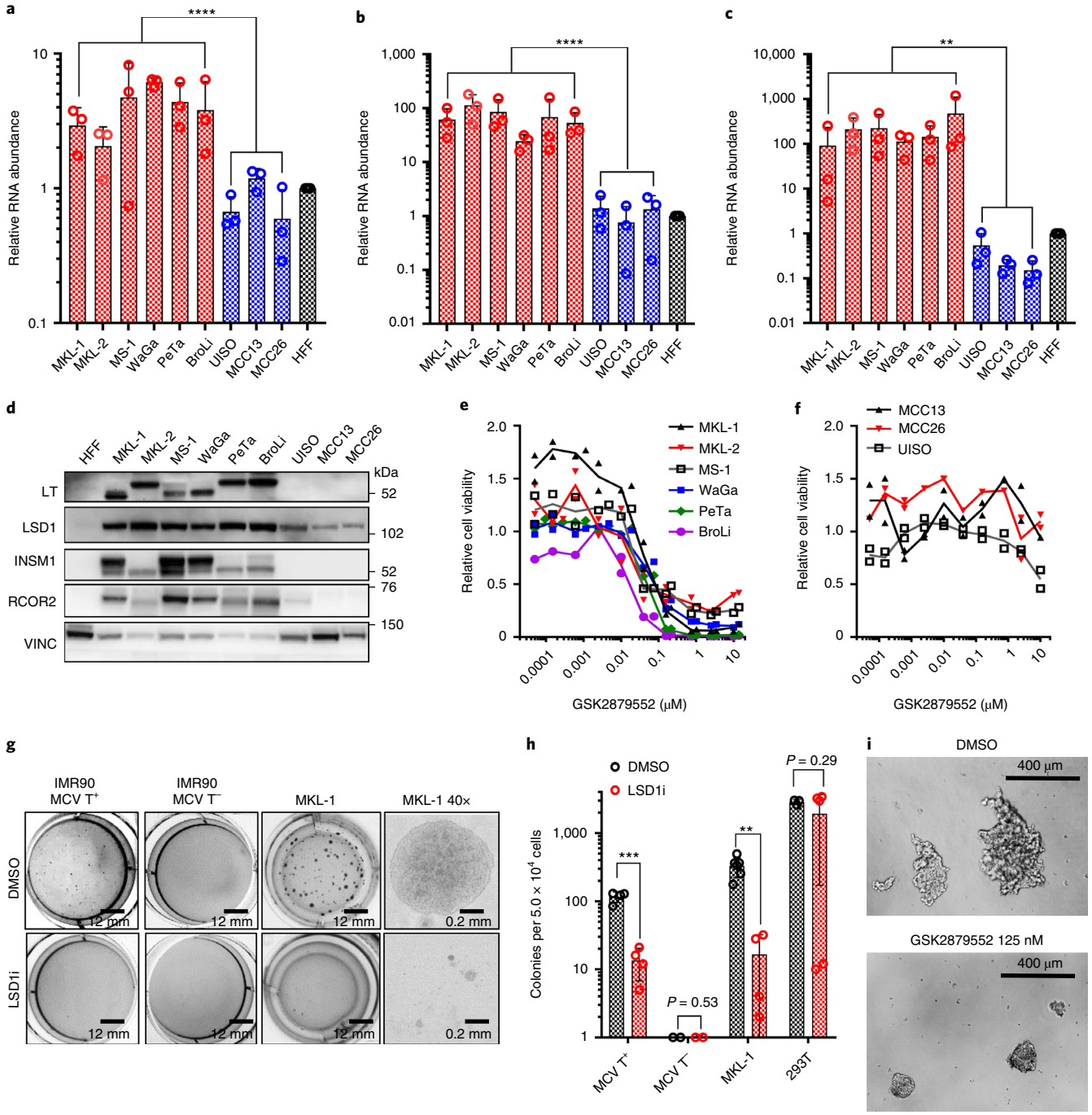

Fig. 2 | LSD1 inhibition abrogates MCV T antigen-dependent transformation. a–c, RT-qPCR of six virus-positive MCC lines (MKL-1, MKL-2, MS-1, WaGa, PeTa and BroLi), three virus-negative MCC lines (UISO, MCC13 and MCC26) and one primary human cell line (HFFs) was performed in triplicate. The levels of *LSD1* (**a**), *RCOR2* (**b**) and *INSM1* (**c**) are shown. The signals were normalized to the geomean of three loading controls (18S ribosomal RNA, *RPLP0* and β-actin (*ACTB*)). The data are shown as the means of $n = 3$ biologically independent samples ± s.d. (two-sided *t*-test). **d**, MCV-positive MCC cell lines express abundant levels of INSM1 and RCOR2. The experiment was performed at least three times. **e**,**f**, Virus-positive (**e**) but not virus-negative (**f**) MCC cell lines are sensitive to LSD1 inhibition. The cells were treated with various concentrations of the LSD1 inhibitor GSK2879552 for 12 d. The CellTiter-Glo assay measured relative viability. The data are presented as the means of $n = 3$ biologically independent samples. **g**, Anchorage-independent growth of IMR90 PHL cells expressing MCV T antigens and MKL-1 MCC cells with an LSD1 inhibitor (GSK-LSD1; 0.1 μM) showed that colony formation of normal cells by MCV T antigens and MCC maintenance was dependent on LSD1 activity. **h**, Quantification of the number of soft agar colonies (see **g**). The data are presented as the means of $n = 4$ biologically independent samples ± s.d. (two-sided *t*-test). **i**, MKL-1 cells were treated with GSK2879552 for 8 d. The results are representative of at least five experiments. $^*P < 0.05$; $^{**}P < 0.005$; $^{****}P < 0.00005$. Unprocessed western blots are available as source data for **d**.

LSD1 and RCOR2 ChIP-Seq in the MKL-1 cell line. The SeqPos motif tool revealed that the binding motifs of the basic helix–loop–helix transcription factors ATOH1, OLIG2 and ASCL2 were most significantly enriched (Fig. 4c and Extended Data Fig. 4d)[27]. ATOH1 is a master transcription factor required for normal Merkel cell lineage[28]. Moreover, ATOH1 was significantly more abundant in

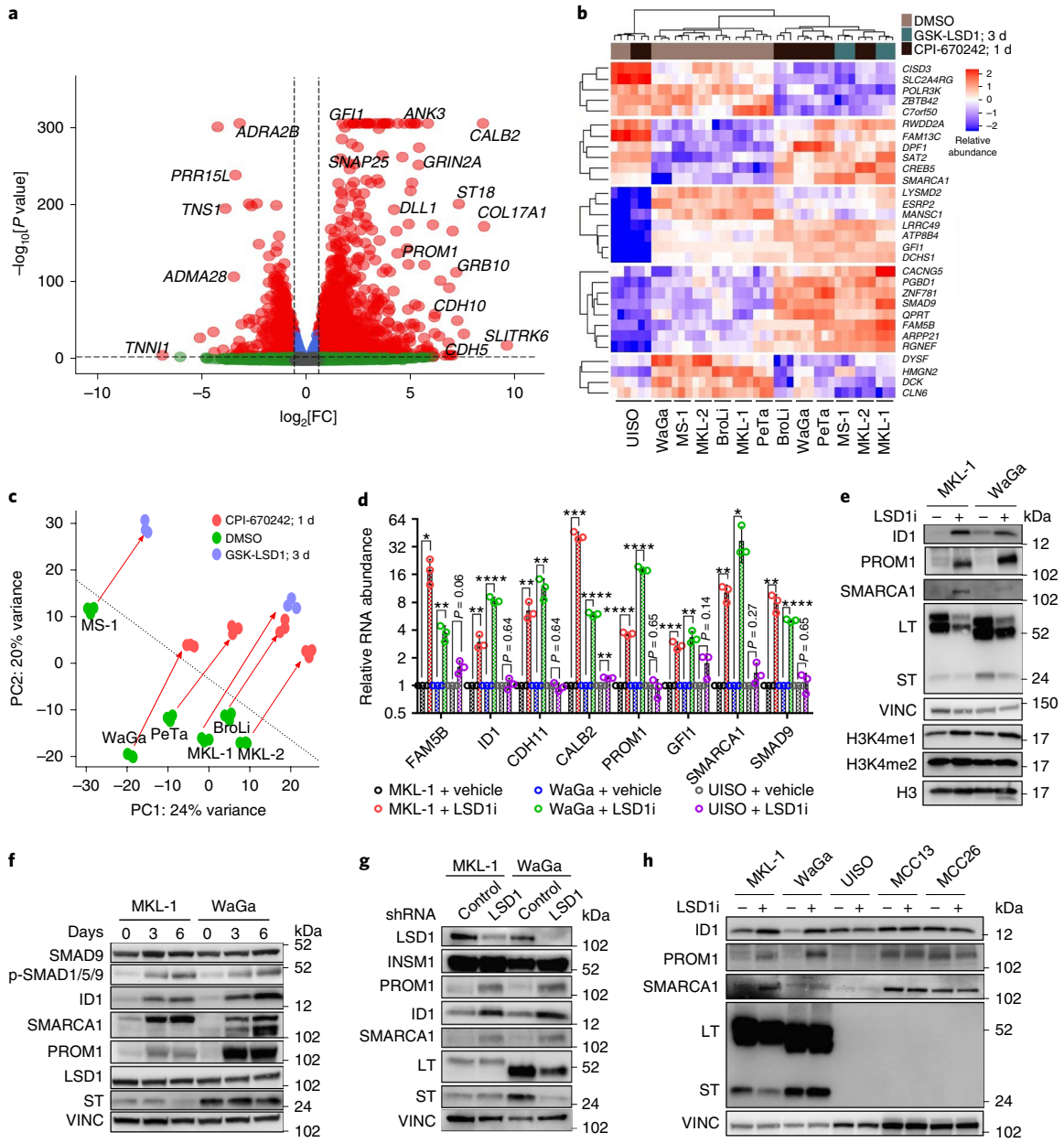

Fig. 3 | RNA-Seq revealed critical gene expression changes during LSD1 inhibition in MCC. a, MKL-1 cells were treated with GSK-LSD1 (0.1 μM) for 3 d and processed for RNA-Seq (NS: not significant; $\log_2$[FC]: fold-change cut-off of 1.5; *P*: *P* value cut-off of 10×10^{-6}). The Wald test was performed using the DEseq2 R package[42] with the *P* values adjusted using the Benjamini–Hochberg method ($n=3$ biologically independent samples). **b**, RNA-Seq of six virus-positive MCC cell lines and one virus-negative UISO cell line treated with LSD1 inhibitors (GSK-LSD1 for 3 d or CPI-670242 for 1 d) ($n=3$ biologically independent samples). **c**, PCA displayed global gene expression changes caused by LSD1 inhibition. d, MKL-1, WaGa and UISO cell lines were treated with GSK-LSD1 (0.05 μM) for 3 d. The signals were normalized to untreated samples and RPLP0 in each sample. The data are presented as the means of $n=3$ biologically independent samples ± s.d. (two-sided *t*-test; $^*P<0.05$; $^{**}P<0.005$; $^{***}P<0.0005$; $^{****}P<0.00005$). **e**, LSD1 inhibition increases global levels of H3K4me1 and LSD1 target genes. MKL-1 and WaGa cells were treated with GSK-LSD1 (0.05 μM) for 6 d and the whole-cell lysates and histone extracts were prepared. Experiments were performed at least three times. **f**, Cells were treated with the LSD inhibitor GSK-LSD1 (0.05 μM) for 3 or 6 d. LSD1 inhibition activates the BMP pathway as assessed by increased levels of phosphorylated SMAD1/5/9 (pSMAD1/5/9). Experiments were performed at least three times. **g**, Cells were transduced with either control or LSD1-targeting shRNA for 6 d and harvested for western blotting. Experiments were performed at least three times. **h**. LSD1 inhibition perturbs gene expression in the virus-positive MCC cell lines but not in the virus-negative MCC cell lines. Cells were treated with GSK-LSD1 (0.05 μM) for 3 d. Experiments were performed at least three times. Unprocessed western blots are available as source data for **e**–**h**.

virus-positive MCC cells compared with virus-negative cells, while small T antigen, MAX and EP400 bound specifically to the ATOH1 promoter (Fig. 1e and Extended Data Fig. 3i).

ChIP-Seq of ATOH1 in MKL-1 cells revealed that LSD1, RCOR2 and ATOH1 bind to an overlapping set of genes (Fig. 4a,b and Extended Data Fig. 4a–c). ATOH1 binding appeared to be centred on transcription start sites (TSSs) of target genes, while LSD1 and RCOR2 peaks were within 500 base pairs (bp) of the TSSs (Fig. 4d,e). The binding of LSD1, RCOR2 and ATOH1 to proximal promoters (≤1 kilobase pair) (15–17%), intragenic regions (~45%)

and distal intergenic regions (~35%) was enriched in similar proportions for each of the three proteins (Fig. 4f and Supplementary Tables 6–8). Pathway analysis of the of LSD1, RCOR2 and ATOH1 peaks revealed that they bind to genes enriched for axon guidance and stem cell pluripotency (Extended Data Fig. 4e).

Next, we sought to determine the effect of LSD1 inhibitors on the DNA occupancy of LSD1, RCOR2 and ATOH1. ChIP-qPCR in untreated MKL-1 cells detected significant enrichment of LSD1, RCOR2 and ATOH1 at the *ID1* and *SMAD9* promoters. Following LSD1 inhibition, enrichment of LSD1 at these target genes, as well as at *ZNF781*, *HES1* and *DLL1*, was markedly decreased (Fig. 4g). In contrast, LSD1 inhibition led to increased ATOH1 enrichment at *ID1* and *SMAD9* (Fig. 4h). This result indicates that LSD1–RCOR2 and ATOH1 compete for binding to a common set of genes.

LSD1 inhibitors have been shown to perturb the neuroendocrine transcription program in small cell lung cancer by disrupting LSD1 interactions with chromatin that are mediated by the SNAG domain protein INSM1 (ref. [10]). In MCC, we determined that LSD1 associates with INSM1 (Fig. 1f and Supplementary Table 4). We performed immunoprecipitation–mass spectrometry (MudPIT) with an INSM1 antibody using MKL-1 cells treated with the LSD1 inhibitor (GSK-LSD1) and found that the INSM1 interaction with LSD1 decreased with inhibitor treatment (Supplementary Table 10). Immunoprecipitation–western blotting experiments confirmed that INSM1 had reduced binding to LSD1 after the inhibitor treatment (Extended Data Fig. 3g,h).

LSD1 inhibition reduces growth of MCC cells in mice and perturbs neuronal gene expression in human and mouse tissues. To identify changes at the protein level with LSD1 inhibition, we performed multiplexed isobaric tag-based profiling[29] of the MKL-1 virus-positive MCC cell line treated with the GSK-LSD1 inhibitor for 8 d. LSD1 inhibition led to major perturbations in protein expression (Fig. 5a). Proteins upregulated by LSD1 inhibition were enriched for pathways in cell adhesion, axonogenesis and neuron differentiation (Extended Data Fig. 5a,b). About 30% of proteins that were significantly increased in response to LSD1 inhibition were also identified as LSD1 targets by the integrated RNA-Seq and ChIP-Seq analysis, including CALB2, PROM1, FAM5B, DLL1 and GFI1 (Extended Data Fig. 3e and Supplementary Table 11).

We tested the efficacy of targeting LSD1 in vivo using MKL-1 and WaGa virus-positive MCC cells grown as xenografts in NOD *scid* gamma (NSG) mice. When the subcutaneous tumours reached 150 mm^3, mice were treated with the CPI-242 LSD1 inhibitor dosed once weekly by oral gavage. LSD1 inhibition significantly decreased the rate of tumour growth in both MCC xenograft models (Fig. 5b and Supplementary Tables 12 and 13).

To explore the tumour response to LSD1 inhibition in vivo, we assessed the proteome of the treated MKL-1 and WaGa xenografts by performing a similar multiplexed isobaric tag-based profiling experiment (Fig. 5c–g, Extended Data Figs. 5c and 6a–d and Supplementary Tables 14–17)[29]. We observed that proteins involved in neuron differentiation, including CNTN2 (contactin 2), NEFL (neurofilament light), NEFM (neurofilament medium) and SYT4 (synaptotagmin 4), were significantly increased in both MKL-1 and WaGa xenografts treated with the LSD1 inhibitor (Fig. 5c). The detection of CNTN2, SYT4, NEFL and NEFM is typically restricted to the brain and some neuronal lineage tissues[30]. Gene Ontology analysis of the proteins upregulated during LSD1 inhibition was enriched for cytoskeleton organization in neuron projections (Fig. 5d). Interestingly, mouse neuronal proteins, including Rph3a (Rabphilin-3A), Nefl and Dclk1 (doublecortin-like kinase 1), also increased during LSD1 inhibition, indicating that LSD1 inhibition affected neuronal differentiation in mouse tissues in the xenograft experiment (Fig. 5f and Extended Data Fig. 5c).

In contrast with the factors upregulated by LSD1 inhibition, proteins with decreased levels were involved in epithelial growth signalling and extracellular organization, including MUC1 (mucin 1), CNPY1 (canopy FGF signalling regulator 1), SPRR1A (small proline-rich protein 1A), CDC6 (cell division cycle 6) and PCOLCE2 (procollagen C-endopeptidase enhancer 2) (Fig. 5e). Mouse proteins that decreased during LSD1 inhibitor treatment of xenografts were enriched for wound healing and inflammatory response pathways, consistent with the observed shrinkage of tumours (Fig. 5g and Extended Data Fig. 5c).

Knockout of ncBAF complex components confers resistance to LSD1 inhibition in MCC. To gain insight into the mechanism of LSD1 inhibition-mediated cell growth inhibition in MCC, we performed a genome-wide CRISPR–Cas9 screen[31]. MKL-1 cells were transduced with human CRISPR–Cas9 knockout pooled lentivirus libraries followed by treatment with 1.5 nM (the concentration for 30% reduction of cell viability (IC_{30})) of GSK-LSD1 or vehicle for 20 d. Transduced cells were collected on days 0 and 20 of treatment and sequenced for short guide RNA (sgRNA) (Fig. 6a,b). Reads from day 20 samples (control and treated) were normalized to those from day 0 samples to identify differentially selected genes (Fig. 6c–e and Supplementary Tables 18–20). Knockout of the positively selected genes (group A: 3,624 genes) promoted proliferation during LSD1 inhibition, whereas knockout of the negatively selected genes (group B: 2,207 genes) augmented LSD1 inhibition in blocking cell growth (Fig. 6d). Lysine methyltransferase 2C (KMT2C (MLL3)) was positively selected during LSD1 inhibition (Fig. 6e,f). KMT2C is the primary mammalian H3K4 mono- and dimethyltransferase involved in the activation of cell type-specific gene expression during differentiation[32]. The positive selection of KMT2C in the resistance screen suggests that it may be a writer of the active histone marks erased by LSD1.

In addition to KMT2C, several components of the ncBAF complex, including *BRD9* and *GLTSCR1* (BICRA), were among the most significant, positively selected genes in the screen (Fig. 6e,f)[16–18]. Other significant, positively selected ncBAF components included *SMARCD1*, *SMARCC1* and *SMARCA2* (Extended Data Fig. 7a).

Fig. 4 | LSD1 and RCOR2 bind to the ATOH1 transcription factor binding motif close to TSSs of genes involved in differentiation pathways. a, Tag heatmaps of LSD1, RCOR2 and ATOH1 ChIP-Seq. The LSD1–RCOR2–ATOH1 overlapping peaks show the factors' shared occupancy in the TSS regions (±4,000 bp). Peaks from two independent replicates of ChIP-Seq were combined, and the shared peaks were determined using BEDtools[43]. **b**, RCOR2, LSD1 and ATOH1 (two biological replicates each: _1 and _2) ChIP-Seq peaks in the *SMAD9*, *HES1* and *ID1* genes are shown. The peaks were visualized with the Integrative Genomics Viewer genome browser[44]. **c**, The SeqPos motif tool[27] was used to determine the LSD1 binding motifs in MKL-1 cells. The binding motifs of ATOH1, OLIG2 and ASCL2 were enriched in the LSD1 ChIP-Seq. **d**,**e**, Peak frequency in the TSS regions revealed that LSD1, RCOR2 and ATOH1 bind close to TSSs. TSS ± 2,000 bp (**d**; promoters) and TSS ± 10,000 bp (**e**; promoters and proximal enhancers) are shown. **f**, ChIP-Seq annotations indicate that LSD1, RCOR2 and ATOH1 bind to shared genomic regions. **g**, ChIP-qPCR of LSD1 in MKL-1 MCC cells, showing that LSD1 enrichment decreases following LSD1 inhibition. MKL-1 cells were treated with GSK-LSD1 for 3 d. The levels of LSD1 binding decreased after treatment with LSD1 inhibitor. The data are presented as the means of $n = 4$ biologically independent samples ± s.d. (two-sided *t*-test). **h**, ChIP-qPCR showing that ATOH1 binds to LSD1 target genes, ID1 and SMAD9. MKL-1 cells were treated with GSK-LSD1 for 3 d and harvested for ChIP with ATOH1. The data are presented as the means of $n = 3$ biologically independent samples ± s.d. (two-sided *t*-test) $^*P < 0.05$; $^{**}P < 0.005$. UTR, untranslated region.

To determine whether BRD9 formed the ncBAF complex in MKL-1 cells, we performed large-scale immunoprecipitation of the endogenous BRD9, followed by MudPIT to identify associated proteins (Fig. 6g and Supplementary Table 21). We observed that BRD9 co-precipitated GLTSCR1 and SMARCA4 and several additional components of the ncBAF complex. This finding was confirmed by western blot in MCC cells (Extended Data Fig. 7b). In contrast, BRD9 did not associate with components restricted to the BAF and PBAF complexes, such as ARID1A, ARID2, PBRM1 and BRD7.

LSD1 and BRD9 regulate an overlapping set of genes in MCC. To assess the role of the ncBAF complex in MCC, we used a bifunctional inhibitor, dBRD9, that selectively degrades BRD9 by bridging the bromodomain and the cereblon (encoded by the *CRBN* gene) E3 ubiquitin ligase complex (Extended Data Fig. 7d)[33]. To determine whether depletion of BRD9 confers resistance to LSD1 inhibition, we treated MKL-1 cells with GSK-LSD1 and dBRD9 or a related BRD9 inhibitor (BRD9i; BI-7273) without the linker to *CRBN* for 6 d, and measured viability by XTT assay (Fig. 7a). The addition of dBRD9 or

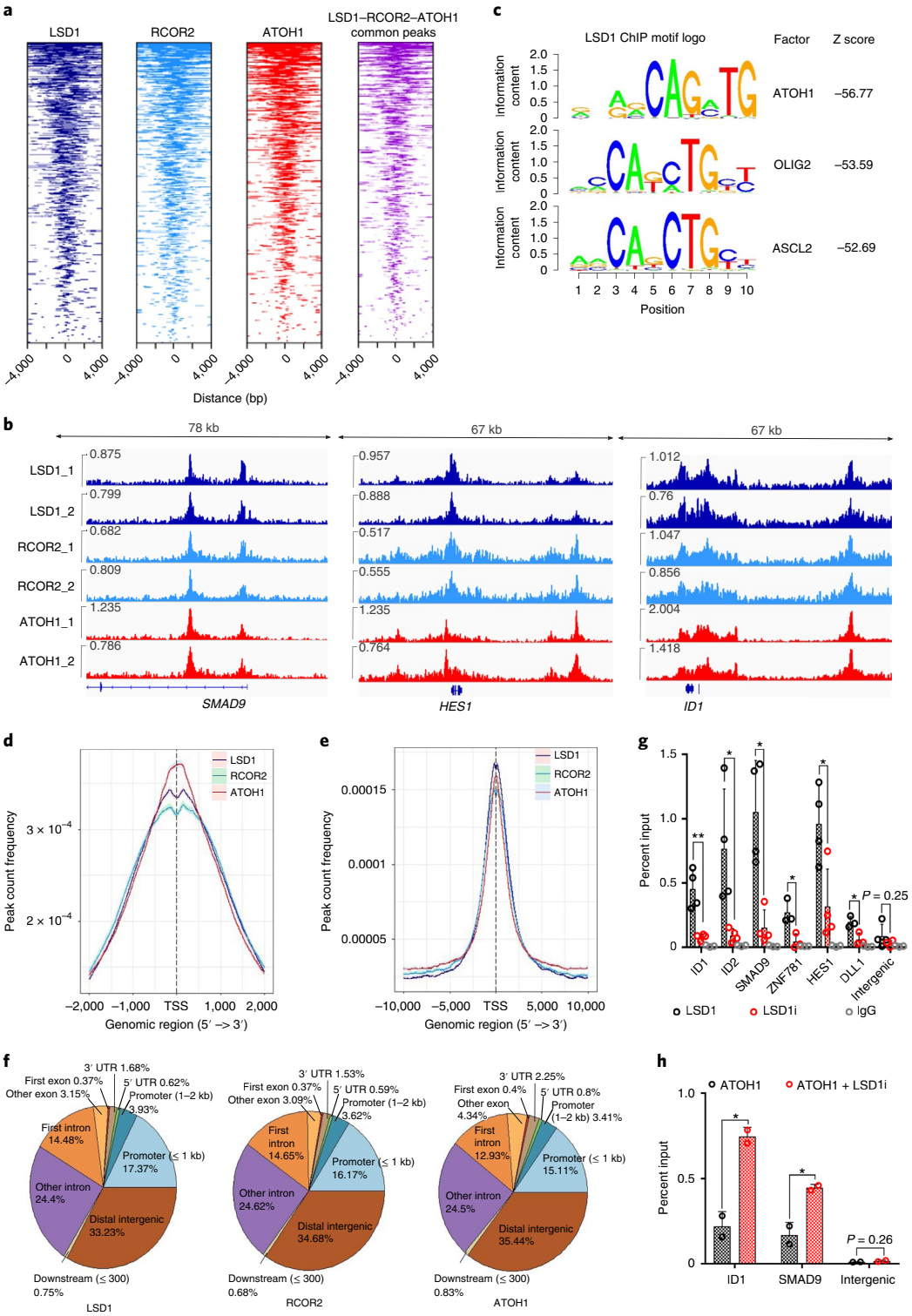

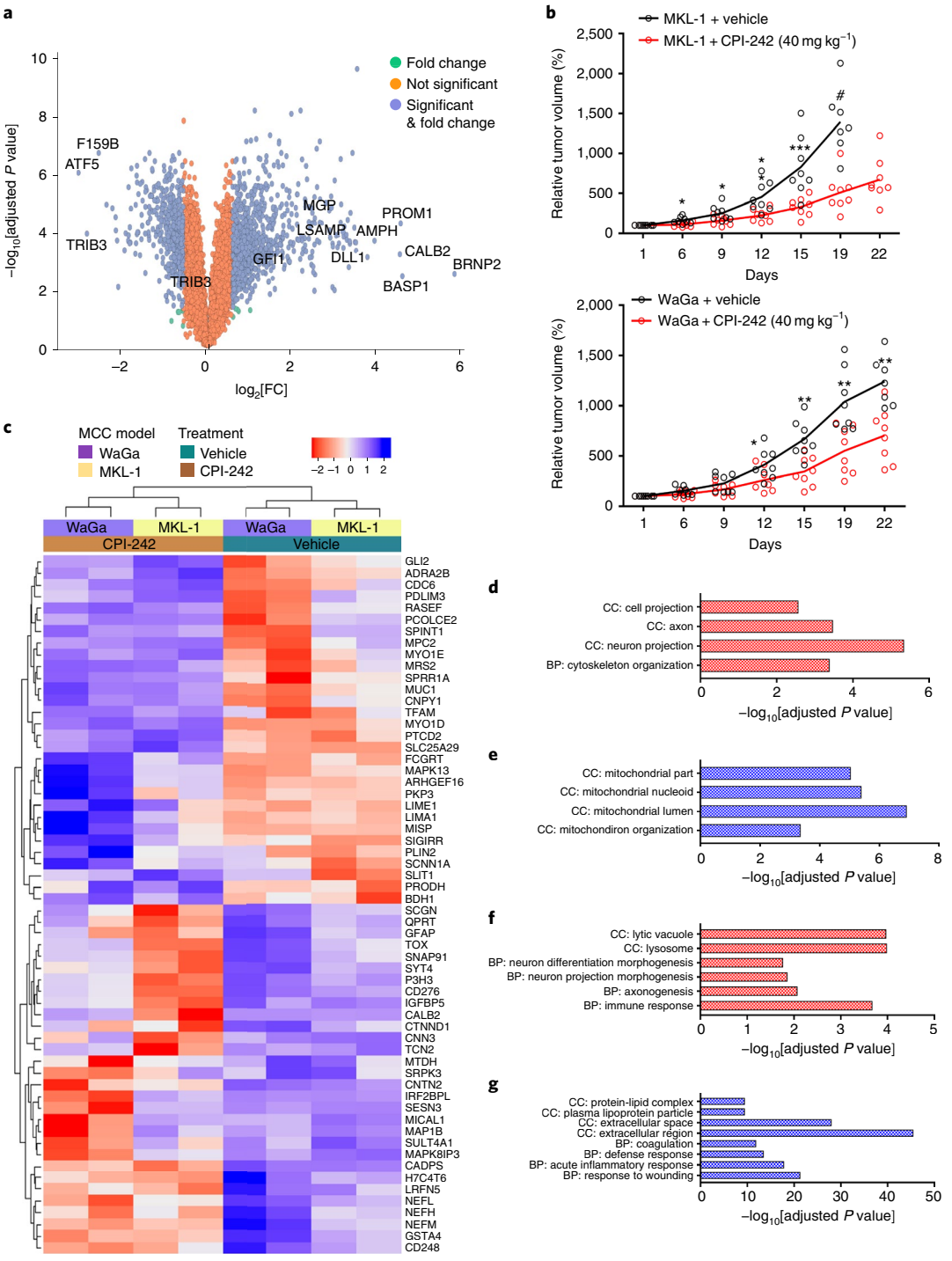

Fig. 5 | Multiplexed isobaric tag-based profiling of the MKL-1 cell line and MCC-derived xenografts revealed that LSD1 inhibition perturbs neuronal gene expression in human and mouse tissues. a. Multiplexed isobaric tag-based profiling of the MKL-1 virus-positive MCC cell line treated with GSK-LSD1 for 8 d displayed global changes in the proteome. Changes in the differentially expressed proteins are shown. Tukey's honest significance test was performed post hoc on peptide-level linear models for each protein and the *P* values were adjusted using the Benjamini–Hochberg method. The levels of proteins identified with arrows had a significant fold-change ($n = 5$ biologically independent samples). Blue represents $\log_2[FC] > 1.5$; light blue represents $\log_2[FC] > 1.5$ and FDR < 0.05; pink represents no significant change. **b**, MKL-1 and WaGa MCC cell lines grown as xenografts in NSG mice had reduced growth rates with LSD1 inhibitors. The hashtag indicates that day 22 data were not plotted as only three out of eight mice were still alive. The data are presented as the means of $n = 8$ independent animals (two-sided *t*-test; $^*P < 0.05$; $^{**}P < 0.005$; $^{***}P < 0.0005$) (see Supplementary Tables 12 and 13). **c**–**g**, Tumours from the MKL-1 or WaGa model ($n = 2$ independent animals per group per model) were harvested 6 h after the last dose for the TMT10plex isobaric tag-labelling quantitative mass spectrometry experiment. The heatmap in **c** shows the relative abundance of the 30 most upregulated and 30 most downregulated human (tumour) proteins after treatment (see Methods). For **d**–**g**, selected GOTERM biological process (BP) and cell compartment (CC) values of $-\log_{10}$[Bonferroni-adjusted *P* values] for the pathways enriched with the top 100 most differentially expressed upregulated human proteins (**d**), downregulated human proteins (**e**), upregulated mouse proteins (**f**) and downregulated mouse proteins (**g**) are shown. The clustering test was implemented using kappa statistics[45].

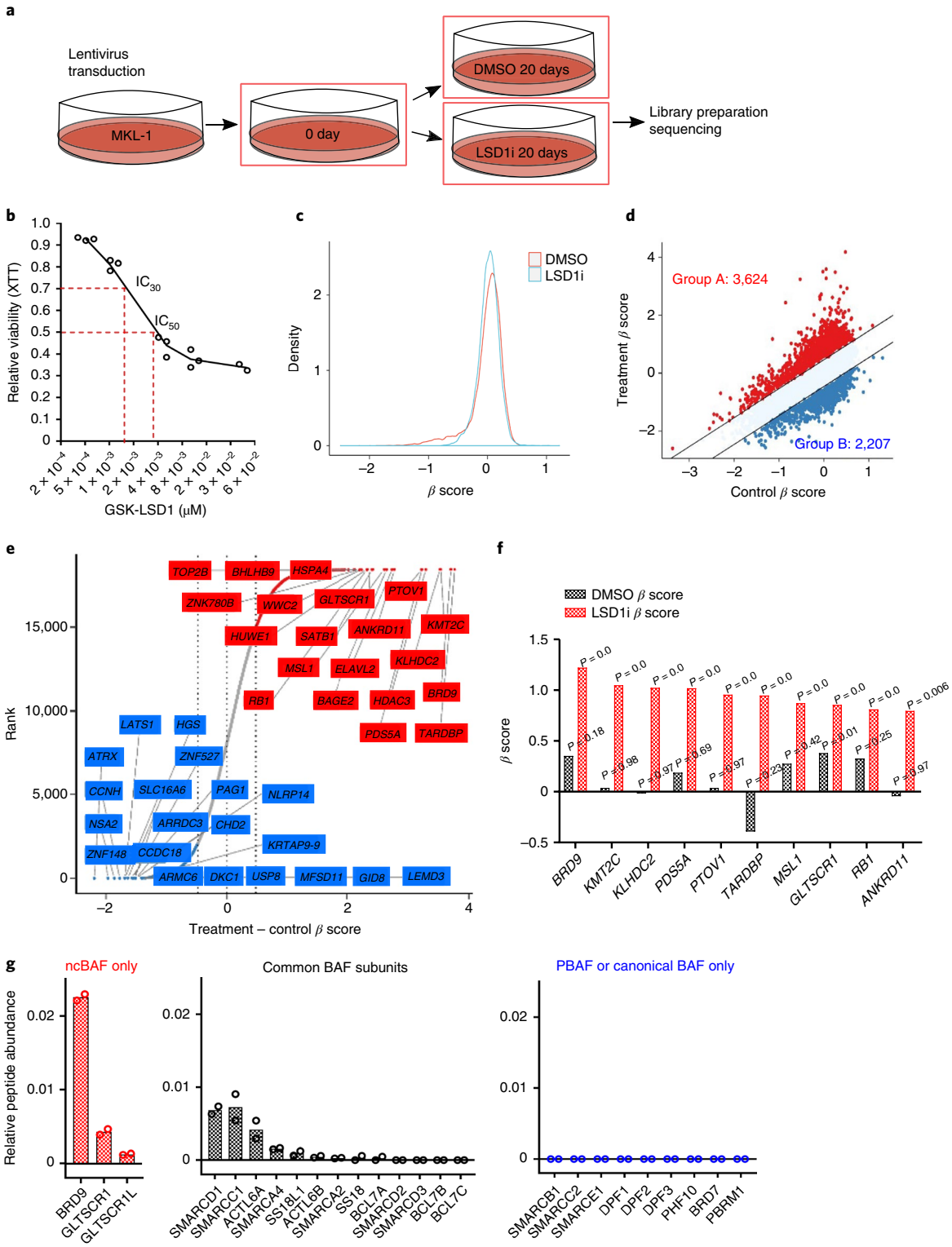

Fig. 6 | CRISPR–Cas9 genome-wide screening for resistance to LSD1 inhibitors creates positive pressure for the loss of ncBAF complex components. **a**, Experimental design for CRISPR–Cas9 screening. **b**, MKL-1 cells display sensitivity to GSK-LSD1 in a dose-dependent manner. IC_{30} (1.5 nM) and IC_{50} values (4 nM) are shown. For the CRISPR–Cas9 screen, IC_{30} was used. The data are presented as the means of $n = 3$ biologically independent samples. **c**, MAGeCKFlute normalization results in a normal distribution of β scores (selection) for the control and treated (LSD1i) samples (1.5 nM for 20 d)[46]. **d**, Genes positively (group A) or negatively selected (group B) during the CRISPR screen were determined based on the β scores of the control (DMSO; 20 d) and treated samples (LSD1i; 20 d; IC_{30}). **e**, Gene ranks based on the β scores showed positively and negatively selected genes. The top 20 genes in each group are shown. The dashed lines are the thresholds set to determine the significant differentially selected genes. **f**, Top ten most significantly positively selected genes in the LSD1i screen. The *P* values were estimated using the MAGeCK-MLE model and were adjusted by FDR[46]. **g**, Two independent BRD9 MudPIT analyses in MKL-1 cells identified ncBAF complex components, including GLTSCR1 and GLTSCR1L1, that were not included as canonical BAF or PBAF complex-specific components. dNSAF (distributed normalized spectral abundance factor) values are shown (see Methods).

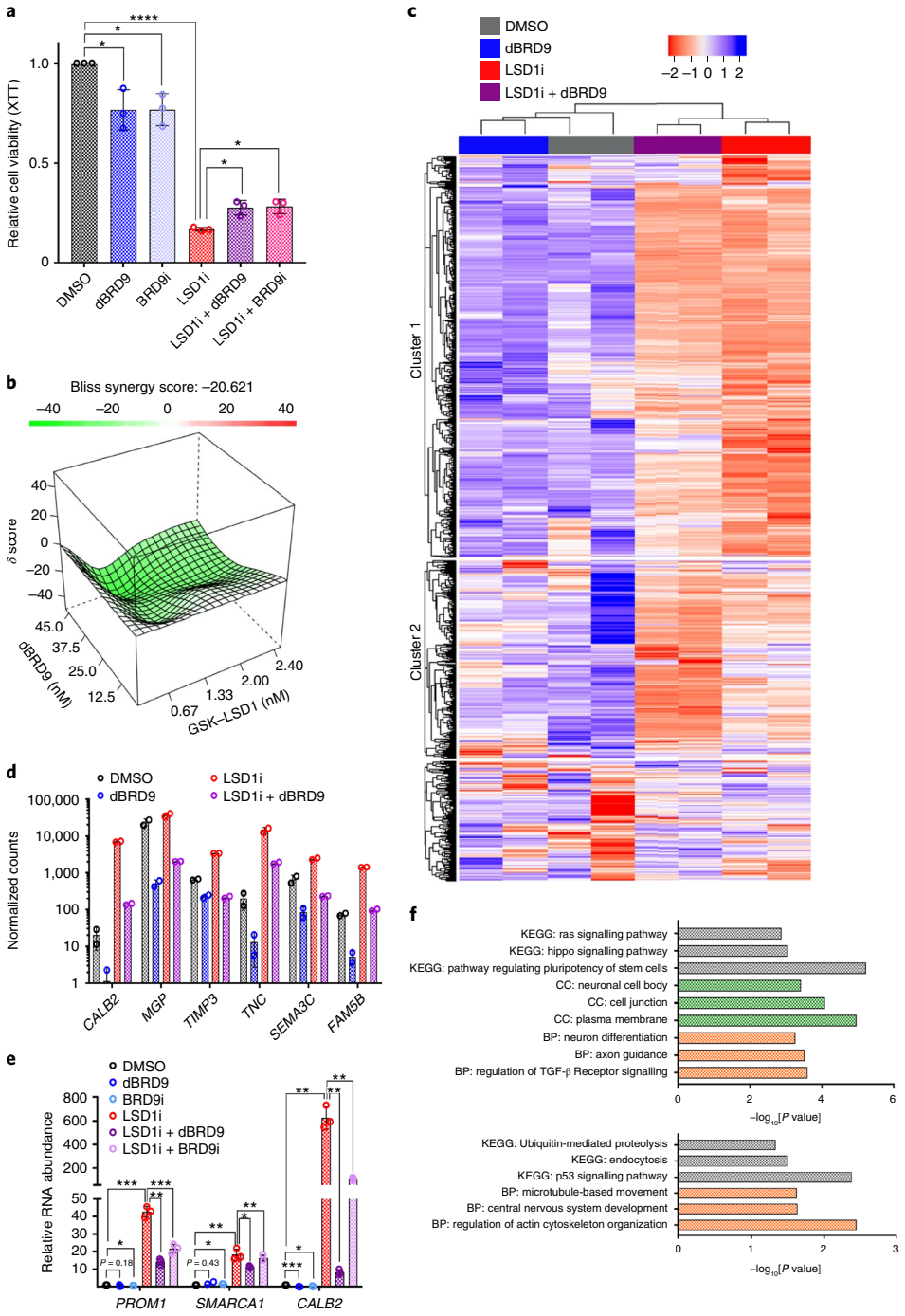

Fig. 7 | LSD1 and BRD9 regulate an overlapping set of genes in MCC. a, BRD9 degradation or inhibition partially rescues the reduced cell viability caused by LSD1 inhibition in MCC. MKL-1 cells were treated with DMSO, LSD1i (0.1 μM), dBRD9 (1 μM), BRD9i (BI-7273; 1 μM) or a combination of LSD1i with dBRD9 or BRD9i for 6 d. The XTT assay was used to measure relative cell viability. The data are presented as the means of $n = 3$ biologically independent samples ± s.d. (two-sided *t*-test). **b**, MKL-1 cells were treated with varying doses of GSK-LSD1 or dBRD9 for 6 d. SynergyFinder[47] was used to calculate negative synergy (rescue) scores. **c**, RNA-Seq was performed with two replicates of MKL-1 cells treated with DMSO, LSD1i (0.1 μM), dBRD9 (0.1 μM) or both GSK-LSD1 and dBRD9 for 6 d ($n = 2$ biologically independent samples). The heatmap shows the expression changes in 1,111 genes induced by LSD1i in six virus-positive MCC cell lines (FDR < 0.1; Fig. 3a–c). **d**, DESeq2 counts of selected LSD1 target genes are shown. Multiple *t*-tests were performed and the *P* values were adjusted by FDR (see Supplementary Table 24). The data are presented as the means of $n = 2$ biologically independent samples ± s.d. **e**, Selected GOTERM biological processes, cellular components or Kyoto Encyclopedia of Genes and Genomes (KEGG) $-\log_{10}$[*P* values] for the pathways enriched with the cluster 1 and 2 genes. The clustering test was implemented using kappa statistics[45] ($n = 2$ biologically independent samples). **f**, MKL-1 cells were treated with DMSO, LSD1i (0.05 μM), dBRD9 (1 μM), BRD9i (BI-7273; 1 μM), LSD1i + dBRD9 or LSD1i + BRD9i for 3 d. The signals were normalized to the DMSO-treated sample and RPLP0. Top, cluster 1 pathways; bottom, cluster 2 pathways; gray, KEGG pathway; green, GOTERM cell compartment (CC); orange, GOTERM biological process (BP). The data are presented as the means of $n = 3$ biologically independent samples ± s.d. *P* values were adjusted using the Bonferroni method (two-sided *t*-test). $^*P < 0.05$; $^{**}P < 0.005$; $^{***}P < 0.0005$; $^{****}P < 0.00005$. TGF-β, transforming growth factor-β.

BRD9i partially rescued the decreased levels of cell viability caused by LSD1 inhibition in MKL-1 cells (Fig. 7a,b and Extended Data Fig. 7c).

Since LSD1 inhibition led to the de-repression of specific genes, we suspected that this de-repression required the ncBAF complex. We tested whether simultaneous inhibition of LSD1 and BRD9 could dampen the expression of the LSD1 target genes. We performed RNA-Seq with MKL-1 cells treated with GSK-LSD1 (LSD1i), dBRD9 or both for 6 d (Fig. 7c–e and Supplementary Table 24). PCA of the RNA-Seq data revealed that inhibition of BRD9 or LSD1 caused global changes in gene expression while dual inhibition led to changes distinct from those of either single treatment alone (Extended Data Fig. 7e). The addition of BRD9 degrader significantly dampened the induction of more than half of LSD1 target genes (cluster 1: 622 out of 1,111 genes) (Fig. 7c,d, Extended Data Fig. 8 and Supplementary Tables 22–24).

We validated by RT-qPCR that levels of *PROM1*, *SMARCA1* and *CALB2* transcripts increased with LSD1 inhibition, and the addition of dBRD9 or BI-7273 dampened this response (Fig. 7e). Also, the shRNA-mediated knockdown of BRD9 led to decreased levels of PROM1, SMARCA1 and ID1 that were increased by LSD1 depletion (Extended Data Fig. 7f). Genes induced by LSD1 inhibition and repressed by dBRD9 were enriched for pathways involved in neuron differentiation and cell morphology changes (Fig. 7f and Supplementary Tables 25 and 26).

BRD9 is required to de-repress the expression of LSD1 target genes during LSD1 inhibition. We hypothesized that BRD9 is required for increasing levels of LSD1 target genes during LSD1 inhibition. To test this possibility, we performed assay for transposase-accessible chromatin sequencing (ATAC-Seq) to determine the chromatin state of MKL-1 MCC cells treated with LSD1 and BRD9 inhibitors. The PCA analysis of the ATAC-Seq peaks revealed distinct patterns of global changes in chromatin states following LSD1 inhibition, BRD9 degradation or both (Fig. 8a). Remarkably, the combination treatment (LSD1i + dBRD9) had a similar shifting pattern to the control, suggesting that BRD9 degradation restored structural changes in chromatin caused by LSD1 inhibition. We observed that ATAC-Seq peaks reside close to the TSSs in control cells, while LSD1 inhibition increased the open chromatin peaks close to the TSSs, and dBRD9 decreased them (Fig. 8b,c and Extended Data Fig. 9a). By comparing the ATAC-Seq peaks, we determined that the peaks gained by adding dBRD9 to LSD1i reside close to the TSSs whose gene products are involved in pathways such as axon guidance and cell-to-cell communications crucial for differentiation and cancer progression (Fig. 8d,e, Extended Data Fig. 9b–d and Supplementary Table 27). A close examination of the ATAC-Seq peaks in the promoters of LSD1 target genes such as *MGP*, *TNC*, *ID1*, *SYT4* and *CALB2*, the expression of which was dampened by the addition of dBRD9, revealed that LSD1 inhibition increased levels of open chromatin in the promoters, and the addition of dBRD9 dampened this increase (Fig. 8f–i and Extended Data Fig. 9e). These results suggest that BRD9 was required to promote the open chromatin states following LSD1 inhibition.

ChIP-qPCR was performed to assess for LSD1 and BRD9 enrichment on LSD1 target genes in MKL-1 cells (Fig. 8j,k). LSD1 binding to the *ID1*, *ID2*, *SMAD9* and *ZNF781* genes decreased after 3 d of LSD1 inhibition, whereas BRD9 enrichment increased significantly. This observation indicates that as LSD1 left from chromatin, BRD9 (presumably in the ncBAF complex) was recruited to these sites. Together with the ATAC-Seq results, these findings indicate that BRD9 and the ncBAF complex are required for de-repressing the expression of a subset of LSD1 target genes during LSD1 inhibition.

Discussion

Here, we report that MCV small T antigen generates an essential dependence on LSD1 activity through transactivation of LSD1 complex components, leading to repression of multiple LSD1–RCOR2–INSM1 target genes that were in turn activated by the ncBAF complex (Extended Data Fig. 9f). Through a comprehensive targetome analysis integrating RNA-Seq, ChIP-Seq, ATAC-Seq and quantitative mass spectrometry, we established that LSD1 inhibition leads to increased expression of genes involved in neuron differentiation. Our findings support a specific role for LSD1 in repressing BMP signalling, which was previously linked to fate specification of neurons and skin cells[34]. Our results are consistent with the finding that keratin 14-driven overexpression of BMP in skin dampens Merkel cell development[35]. LSD1 repression of BMP signalling may also inhibit MCC differentiation that, in turn, regulates neuronal gene expression.

It is important to note that MYCL and the EP400 complex mediate MCV small T antigen oncogenic transformation and LSD1 expression. In this context, the small T antigen–MYCL–EP400 complex represses developmentally related genes by transactivation of the LSD1–RCOR2–INSM1 complex. The MYC and MYCN paralogues of MYCL have been reported to repress specific gene targets by binding directly to a repressor such as MIZ-1 (ZBTB17) or G9a (EHMT2), or by transactivation of a repressor such as EZH2, which in turn represses specific gene targets[36,37]. Here, we find that MYCL functions to indirectly repress a specific set of developmental genes through the LSD1–RCOR2–INSM1 complex. This activity does not exclude the possibility that MYCL may have additional associated repressor activities mediated by MIZ-1, G9a and EZH2.

We observed that DNA bindings of LSD1 and ATOH1 co-localize in proximity to LSD1 target genes. ATOH1 is the master transcription factor for Merkel cell specification[28]. In this role, ATOH1 may act as a pioneer factor to make active transcription sites accessible for other transcription factors, while LSD1 serves to repress specific genes in these sites based on cellular needs.

Fig. 8 | BRD9 is required to de-repress the expression of LSD1 target genes. a–i. Inhibition of LSD1 and BRD9 alters the chromatin accessibility of an overlapping set of genes in an antagonistic manner. Two biological replicates of ATAC-Seq with MKL-1 cells treated with DMSO (control), LSD1i (0.1 μM), dBRD9 (0.1 μM) or LSD1i + dBRD9 for 3 d were performed. **a**, PCA plot displaying global changes in chromatin accessibility following the mentioned treatments. **b**, Peak count frequencies in the TSSs (±2,000 bp) for the indicated conditions. The shaded areas represent 95% confidence intervals. **c**, Peak count frequencies of ATAC-Seq for the indicated conditions (TSSs ± 500 bp). **d**, Frequencies of the differentially enriched peaks between LSD1i and LSD1i + dBRD9. 'Combo gained' displays the frequencies of peaks gained in the LSD1i + dBRD9 combination compared with LSD1i, whereas 'combo lost' shows the frequencies of peaks lost in the combination. **e**, GOTERM biological process pathways enriched with the genes annotated with combo gained ($n = 358$) and combo lost peaks ($n = 431$). The enrichment test was performed on hypergeometric distribution using the clusterProfiler R package[48] and the *P* values were adjusted by FDR[48]. **f**,**g**, DESeq2 normalized counts of *MGP* (**f**) and *TNC* (**g**) from the RNA-Seq of MKL-1 cells treated with DMSO, LSD1i (0.1 μM), dBRD9 (0.1 μM) or LSD1i + dBRD9 (Fig. 7c–e). Differentially expressed genes were found by comparing each condition with DESeq2 (ref. [42]) and *P* values were adjusted using the Benjamini–Hochberg method. **h**,**i**, ATAC-Seq peaks in the promoters of *MGP* (**h**) and *TNC* (**i**) under the indicated conditions with two biological replicates (_1 and _2). The *y* axis spans 0 to 58 in **h** and 0 to 80 in **i**. **j**,**k**, ChIP-qPCR results revealing that LSD1 binding decreases (**j**), whereas BRD9 binding increases (**k**) during LSD1 inhibition. MKL-1 cells were treated with GSK-LSD1 for 3 d. The data are presented as the means of $n = 3$ biologically independent samples ± s.d. (two-sided *t*-test). $^{*}P < 0.05$; $^{**}P < 0.005$; $^{***}P < 0.0005$. cAMP, cyclic AMP; cGMP, cyclic GMP; ECM, extracellular matrix; PKG, cGMP-dependent protein kinase..

We found that all tested virus-positive (but not virus-negative) MCC cell lines responded to LSD1 inhibition. To understand the mechanism of LSD1 inhibition, we determined that the ncBAF chromatin remodelling complex was required to de-repress LSD1 target genes. Inhibition of BRD9—a core component of ncBAF—rescued the loss of cell viability caused by LSD1 inhibition. Loss of ncBAF or its downstream target genes may serve as a mechanism of resistance for targeting LSD1 in neuroendocrine cancers.

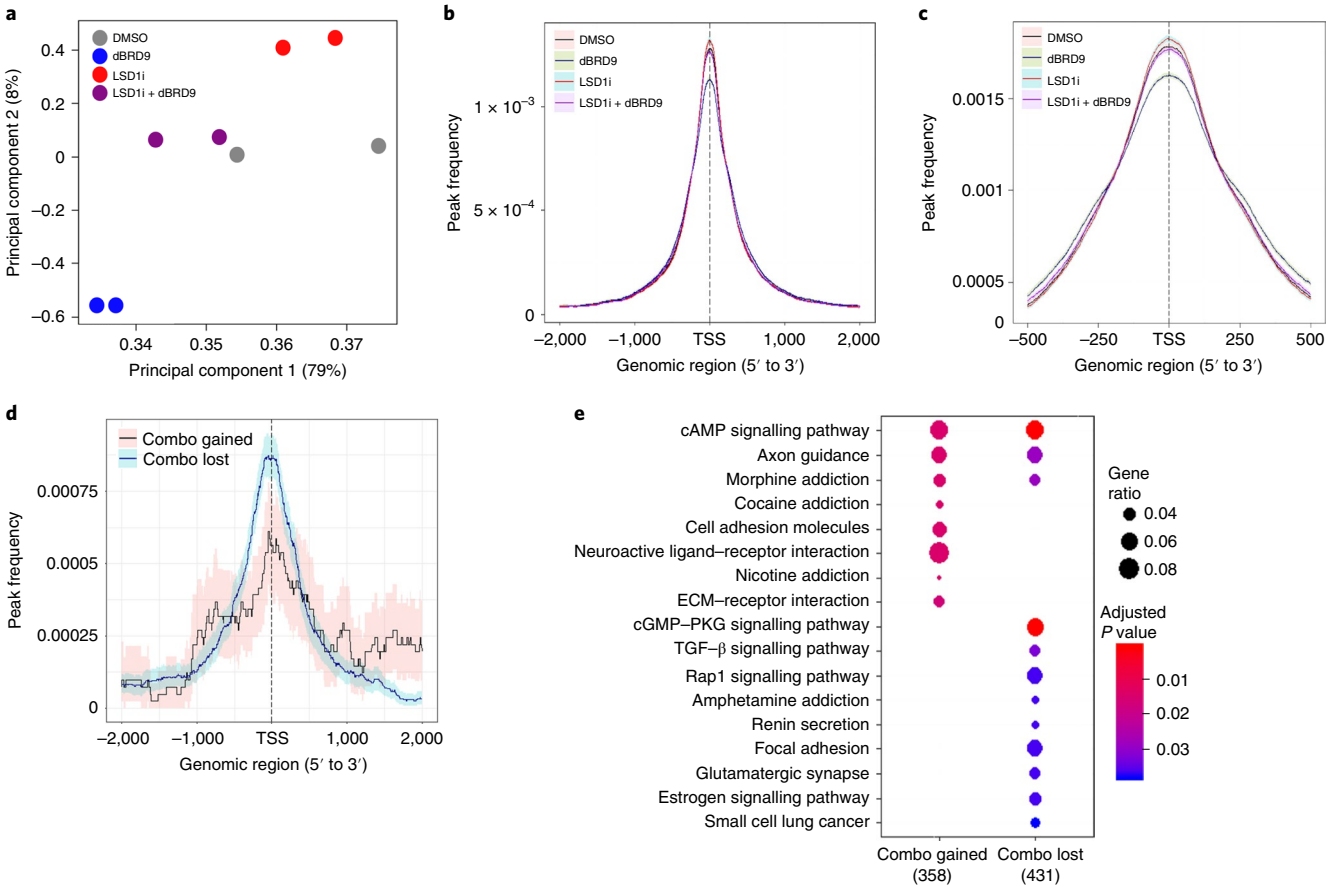

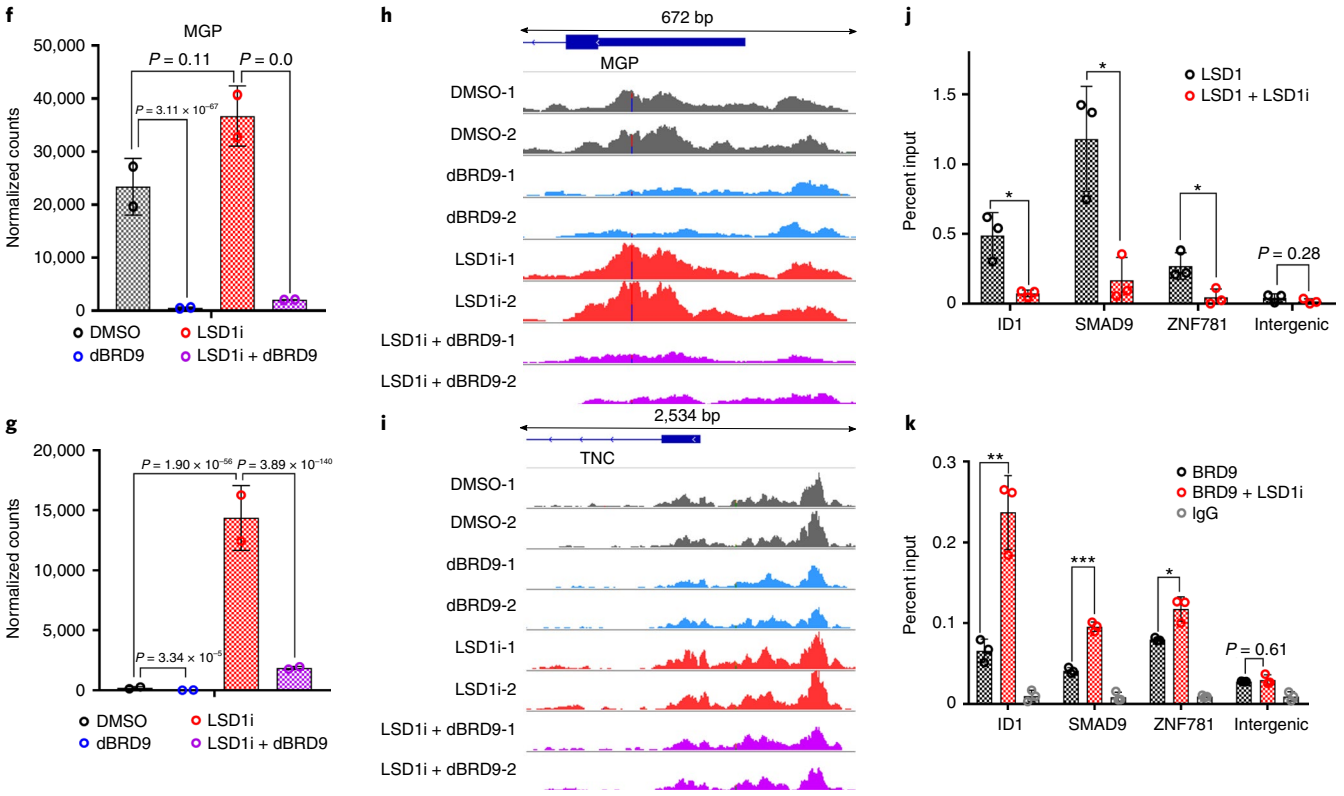

The role of ncBAF in cancer is largely unknown. Perturbation of canonical BAF complexes (that is, the SMARCB1 subunit) generates a dependency on BRD9 in synovial sarcoma[18,38]. In contrast, in cancers with SF3B1 mutations, loss of BRD9 by mis-splicing promotes proliferation, suggesting a tumour suppressor role for BRD9 (ref. [19]).

One promising LSD1 combination therapy may involve immunotherapy. A recent report indicated that LSD1 depletion enhanced programmed death-ligand 1 (CD274) checkpoint blockade in mouse melanoma by increasing type 1 interferon response and anti-tumour T cell infiltration[39]. Historically, therapeutic options for MCC have been limited to surgery, radiation and cytotoxic chemotherapy, although several recent reports showed response rates as high as 62% to checkpoint blockade therapy with programmed cell death protein 1 and programmed death-ligand 1 inhibitors[40]. A strategy combining checkpoint blockade therapy and LSD1 inhibition may prove to be a useful therapeutic strategy for MCC and other cancers.

Online content

Any methods, additional references, Nature Research reporting summaries, source data, extended data, supplementary information, acknowledgements, peer review information; details of author contributions and competing interests; and statements of data and code availability are available at https://doi.org/10.1038/s41556-020-0503-2.

Received: 27 February 2019; Accepted: 4 March 2020;
Published online: 13 April 2020

References

1. Shuda, M. et al. T antigen mutations are a human tumor-specific signature for Merkel cell polyomavirus. *Proc. Natl Acad. Sci. USA* **105**, 16272–16277 (2008).
2. Shuda, M., Kwun, H. J., Feng, H., Chang, Y. & Moore, P. S. Human Merkel cell polyomavirus small T antigen is an oncoprotein targeting the 4E-BP1 translation regulator. *J. Clin. Invest.* **121**, 3623–3634 (2011).
3. Harms, P. W. et al. The distinctive mutational spectra of polyomavirus-negative Merkel cell carcinoma. *Cancer Res.* **75**, 3720–3727 (2015).
4. Moll, I., Kuhn, C. & Moll, R. Cytokeratin 20 is a general marker of cutaneous Merkel cells while certain neuronal proteins are absent. *J. Invest. Dermatol.* **104**, 910–915 (1995).
5. Cheng, J. et al. Merkel cell polyomavirus recruits MYCL to the EP400 complex to promote oncogenesis. *PLoS Pathog.* **13**, e1006668 (2017).
6. Park, D. E. et al. Dual inhibition of MDM2 and MDM4 in virus-positive Merkel cell carcinoma enhances the p53 response. *Proc. Natl Acad. Sci. USA* **116**, 1027–1032 (2018).
7. Shi, Y. et al. Histone demethylation mediated by the nuclear amine oxidase homolog LSD1. *Cell* **119**, 941–953 (2004).
8. Laurent, B. et al. A specific LSD1/KDM1A isoform regulates neuronal differentiation through H3K9 demethylation. *Mol. Cell* **57**, 957–970 (2015).
9. Saleque, S., Kim, J., Rooke, H. M. & Orkin, S. H. Epigenetic regulation of hematopoietic differentiation by Gfi-1 and Gfi-1b is mediated by the cofactors CoREST and LSD1. *Mol. Cell* **27**, 562–572 (2007).
10. Takagi, S. et al. LSD1 inhibitor T-3775440 inhibits SCLC cell proliferation by disrupting LSD1 interactions with SNAG domain proteins INSM1 and GFI1B. *Cancer Res.* **77**, 4652–4662 (2017).
11. McGrath, J. P. et al. Pharmacological inhibition of the histone lysine demethylase KDM1A suppresses the growth of multiple acute myeloid leukemia subtypes. *Cancer Res.* **76**, 1975–1988 (2016).
12. Mohammad, H. P. et al. A DNA hypomethylation signature predicts antitumor activity of LSD1 inhibitors in SCLC. *Cancer Cell* **28**, 57–69 (2015).
13. Sugino, N. et al. A novel LSD1 inhibitor NCD38 ameliorates MDS-related leukemia with complex karyotype by attenuating leukemia programs via activating super-enhancers. *Leukemia* **31**, 2303–2314 (2017).
14. Lee, C. et al. Lsd1 as a therapeutic target in Gfi1-activated medulloblastoma. *Nat. Commun.* **10**, 332 (2019).
15. Kadoch, C. et al. Proteomic and bioinformatic analysis of mammalian SWI/SNF complexes identifies extensive roles in human malignancy. *Nat. Genet.* **45**, 592–601 (2013).
16. Mashtalir, N. et al. Modular organization and assembly of SWI/SNF family chromatin remodeling complexes. *Cell* **175**, 1272–1288.e20 (2018).
17. Alpsoy, A. & Dykhuizen, E. C. Glioma tumor suppressor candidate region gene 1 (GLTSCR1) and its paralog GLTSCR1-like form SWI/SNF chromatin remodeling subcomplexes. *J. Biol. Chem.* **293**, 3892–3903 (2018).
18. Michel, B. C. et al. A non-canonical SWI/SNF complex is a synthetic lethal target in cancers driven by BAF complex perturbation. *Nat. Cell Biol.* **20**, 1410–1420 (2018).
19. Inoue, D. et al. Spliceosomal disruption of the non-canonical BAF complex in cancer. *Nature* **574**, 432–436 (2019).
20. Yang, P. et al. RCOR2 is a subunit of the LSD1 complex that regulates ESC property and substitutes for SOX2 in reprogramming somatic cells to pluripotency. *Stem Cells* **29**, 791–801 (2011).
21. Rush, P. S. et al. Insulinoma-associated 1: a novel nuclear marker in Merkel cell carcinoma (cutaneous neuroendocrine carcinoma). *J. Cutan. Pathol.* **45**, 129–135 (2018).
22. Florens, L. & Washburn, M. P. Proteomic analysis by multidimensional protein identification technology. *Methods Mol. Biol.* **328**, 159–175 (2006).
23. Paoletti, A. C. et al. Quantitative proteomic analysis of distinct mammalian Mediator complexes using normalized spectral abundance factors. *Proc. Natl Acad. Sci. USA* **103**, 18928–18933 (2006).
24. Berrios, C. et al. Merkel cell polyomavirus small T antigen promotes pro-glycolytic metabolic perturbations required for transformation. *PLoS Pathog.* **12**, e1006020 (2016).
25. Sharma, R. et al. Bmp signaling maintains a mesoderm progenitor cell state in the mouse tailbud. *Development* **144**, 2982–2993 (2017).
26. Wang, S. et al. Target analysis by integration of transcriptome and ChIP-Seq data with BETA. *Nat. Protoc.* **8**, 2502–2515 (2013).
27. Zhu, L. J. et al. ChIPpeakAnno: a Bioconductor package to annotate ChIP-Seq and ChIP-chip data. *BMC Bioinformatics* **11**, 237 (2010).
28. Wright, M. C. et al. Unipotent, *Atoh1*$^{+}$ progenitors maintain the Merkel cell population in embryonic and adult mice. *J. Cell Biol.* **208**, 367–379 (2015).
29. Paulo, J. & Gygi, S. P. Isobaric tag-based protein profiling of a nicotine-treated alpha7 nicotinic receptor-null human haploid cell line. *Proteomics* **18**, e1700475 (2018).
30. Fagerberg, L. et al. Analysis of the human tissue-specific expression by genome-wide integration of transcriptomics and antibody-based proteomics. *Mol. Cell. Proteomics* **13**, 397–406 (2014).
31. Dhanjal, J. K., Radhakrishnan, N. & Sundar, D. Identifying synthetic lethal targets using CRISPR/Cas9 system. *Methods* **131**, 66–73 (2017).
32. Lee, J.-E. et al. H3K4 mono- and di-methyltransferase MLL4 is required for enhancer activation during cell differentiation. *eLife* **2**, e01503 (2013).
33. Remillard, D. et al. Degradation of the BAF complex factor BRD9 by heterobifunctional ligands. *Angew. Chem.* **56**, 5738–5743 (2017).
34. Huelsken, J., Vogel, R., Erdmann, B., Cotsarelis, G. & Birchmeier, W. β-catenin controls hair follicle morphogenesis and stem cell differentiation in the skin. *Cell* **105**, 533–545 (2001).
35. Guha, U. et al. Target-derived BMP signaling limits sensory neuron number and the extent of peripheral innervation in vivo. *Development* **131**, 1175–1186 (2004).
36. Tu, W. B. et al. MYC interacts with the G9a histone methyltransferase to drive transcriptional repression and tumorigenesis. *Cancer Cell* **34**, 579–595.e8 (2018).
37. Varlakhanova, N., Cotterman, R., Bradnam, K., Korf, I. & Knoepfler, P. S. Myc and Miz-1 have coordinate genomic functions including targeting Hox genes in human embryonic stem cells. *Epigenetics Chromatin* **4**, 20 (2011).
38. Brien, G. L. et al. Targeted degradation of BRD9 reverses oncogenic gene expression in synovial sarcoma. *eLife* **7**, e41305 (2018).
39. Sheng, W. et al. LSD1 ablation stimulates anti-tumor immunity and enables checkpoint blockade. *Cell* **174**, 549–563.e19 (2018).
40. Nghiem, P. T. et al. PD-1 blockade with pembrolizumab in advanced Merkel-cell carcinoma. *N. Engl. J. Med.* **374**, 2542–2552 (2016).
41. Kent, W. J. et al. The human genome browser at UCSC. *Genome Res.* **12**, 996–1006 (2002).
42. Love, M. I., Huber, W. & Anders, S. Moderated estimation of fold change and dispersion for RNA-Seq data with DESeq2. *Genome Biol.* **15**, 550 (2014).
43. Quinlan, A. R. & Hall, I. M. BEDTools: a flexible suite of utilities for comparing genomic features. *Bioinformatics* **26**, 841–842 (2010).
44. Robinson, J. T. et al. Integrative genomics viewer. *Nat. Biotechnol.* **29**, 24–26 (2011).
45. Huang, D. Wa. W., Sherman, B. T. & Lempicki, R. A. Systematic and integrative analysis of large gene lists using DAVID bioinformatics resources. *Nat. Protoc.* **4**, 44–57 (2009).
46. Zhang, W. & Wang, B. MAGeCKFlute: Integrative analysis pipeline for pooled CRISPR functional genetic screens. R package version 1.1.8 (2018).
47. Ianevski, A., He, L., Aittokallio, T. & Tang, J. SynergyFinder: a web application for analyzing drug combination dose–response matrix data. *Bioinformatics* **33**, 2413–2415 (2017).
48. Yu, G., Wang, L.-G. G., Han, Y. & He, Q.-Y. Y. clusterProfiler: an R package for comparing biological themes among gene clusters. *OMICS* **16**, 284–287 (2012).

Methods

Plasmids, cells and cell culture. The expression vectors included pLIX402 inducible empty vector and pLenti CMV Blast empty vector (w263–1), which were gifts from D. Root (41394; Addgene) and E. Campeau (17486; Addgene), respectively. Lentiviral packaging plasmid psPAX2 and envelope plasmid pMD2.G were gifts from D. Trono (12260 and 12259; Addgene). The shRNA clone (number 43; CAGGAGAAGCTGCTGGTATCA) targeting KDM1A was obtained from Cellecta and was carried in the Cellecta third-generation lentiviral plasmid pRSI-U6wt-sh-cPPT-UbiC-zsG-2A-Puro. Generation of the shRNA clones for EP400 was described by Cheng et al.[5]. The shRNA clones targeting RCOR2 (HsSH00209621 and HsSH00209662) and BRD9 (HsSH00206761 and HsSH00206889) were obtained from the Harvard Plasmid Database.

In generating cell lines stably expressing these constructs, IMR90 human lung fibroblast cells and MKL-1 MCC cells were transduced using a three-vector lentivirus transduction system[5]. MCC cell lines were gifts from M. Shuda (University of Pittsburgh), J. Becker (Medical University of Graz) and R. Houben (University of Wuerzburg). 293T and IMR90 cells were obtained from the American Type Culture Collection. The generation of MKL-1 MCC cell lines with inducible expression of shRNA, and IMR90 transformation using p53DD, MYCL and hTERT constructs were described previously[5,24]. IMR90 cells and primary HFFs were cultured in Dulbecco's modified Eagle's medium supplemented with 15% foetal bovine serum (FBS), antibiotics and non-essential amino acids, and MCC cell lines were grown in RPMI medium supplemented with 10% FBS and antibiotics.

Cell viability assay and anchorage-independent growth assay. GSK-LSD1 (SML1072; Sigma–Aldrich), GSK2879552 (A-1385; Active Biochem), CPI-242 and other LSD1 inhibitors (Constellation Pharmaceuticals), dBRD9 (a gift from J. Qi at the Dana-Farber Cancer Institute (DFCI)) and BI-7273 (20311; Cayman Chemical) were reconstituted in dimethyl sulfoxide (DMSO) and added directly to culture media. CPI-242 is an orally available, small-molecule, covalent styrenylcyclopropane inhibitor of LSD1. The structure and activity of this molecule will be covered in a future paper (V. Gehlling et al., manuscript in preparation).

CPI-670242 and other LSD1 inhibitors were arrayed in a ten-point dilution series on the plates (10 μM maximum concentration) before the addition of cells. Cultures were split every fourth day, an aliquot was removed for viable cell counts and the remainder was re-plated at a dilution of ~1:4 into compound-arrayed plates. Cell viability assays were performed using a Cell Proliferation Kit II (XTT) (Roche) or CellTiter-Glo luminescent cell viability assay (Promega) according to the manufacturers' instructions. GraphPad Prism 6 (GraphPad Software) was used for curve fitting and the determination of GI_{50} values. Synergy testing was performed using SynergyFinder[47]. Anchorage-independent growth was performed as described[24] using six-well dishes with SeaPlaque Agarose (Lonza) at concentrations of 0.3% for the top layer and 0.6% for the bottom layer. Agarose was diluted with 2× MEM (Gibco) supplemented with 2× GlutaMAX (Gibco), 2× penicillin-streptomycin (Gibco) and 30% FBS. IMR90 cells were seeded in triplicate in the top agarose layer. Wells were fed with top agarose twice per week. After 4 weeks, cells were stained with 0.005% crystal violet (Sigma–Aldrich) in phosphate-buffered saline (PBS) and the colonies were counted in a blind manner.

Immunoprecipitation and immunoblotting. Confluent cultures of cells were washed with ice-cold PBS and resuspended in EBC lysis buffer (50 mM Tris (pH 8.0), 150 mM NaCl, 0.5% NP-40, 1:10,000 β-mercaptoethanol and 0.5 mM EDTA) for 10 min on ice and then centrifuged. Clarified lysates were quantified and boiled in Laemmli sample buffer for western blotting or incubated overnight with antibodies and magnetic protein A/G beads (PureProteome magnetic beads; EMD Millipore) for immunoprecipitation. The beads were washed with high-salt EBC buffer (50 mM Tris (pH 8.0), 300 mM NaCl, 0.5% NP-40 and 0.5 mM EDTA) five times and boiled in Laemmli sample buffer before sodium dodecyl sulfate–polyacrylamide gel electrophoresis. The Roeder two-step lysis protocol was modified to prepare histone extracts[49]. Briefly, cytoplasmic fractions were separated in buffer A (10 mM Tris (pH 7.9), 1.5 mM $MgCl_2$, 10 mM KCl, 0.5 mM dithiothreitol and Benzonase) and the nuclear pellets were resuspended in buffer C (20 mM Tris (pH 7.9), 25% glycerol, 1.5 mM $MgCl_2$, 0.42 M NaCl, 0.5 mM dithiothreitol and Benzonase). After clarifying the nuclear fraction, the insoluble nuclear material was sonicated in buffer B (20 mM Tris, (pH 7.9), 1.5 mM $MgCl_2$ and 1 M NaCl) and the clarified extract was combined with the soluble nuclear fraction.

Immunoprecipitation and western blotting were performed with antibodies to LSD1 (2139; Cell Signaling Technology; 1:3,000), INSM1 Mouse (SC-271408; Santa Cruz Biotechnology; 1:250), RCOR2 (23969-1-AP; Proteintech Group; 1:2,000), ID1 (SC-488; Santa Cruz Biotechnology; 1:250), MYCL (14584-1-AP; Proteintech Group; 1:1,000), PROM1 (CD133; 18470-1-AP; Proteintech Group; 1:3,000), SMAD9 (LS-C161303-400; Lifespan Biosciences; 1:1,000), Phospho-Smad1 (Ser463/465), -Smad5 (Ser463/465) or -Smad9 (Ser465/467) (13820T; Cell Signaling Technology; 1:3000), SMARCA1 (9450S; Cell Signaling Technology; 1:3,000), BRD9 (61537; Active Motif Rabbit; 1:3,000), BICRA (GLTSCR1; SC-515086; Santa Cruz Biotechnology; 1:250), Cleaved Notch1 (Val1744) (4147T; Cell Signaling Technology; 1:3,000), HES1 (11988S; Cell Signaling Technology; 1:3,000), H3 (9715; Cell Signaling Technology; 1:3,000), dimethyl-histone H3 (Lys4) (C64G9) (9725; Cell Signaling Technology; 1:3,000), mono-methyl-histone H3 (Lys4) (61634; Active Motif; 1:2,000) and normal Rabbit IgG (2729; Cell Signaling Technology; 1:3,000). Mouse monoclonal antibodies Ab3 and Ab5 (1 mg ml^{-1}; 1:1,000 dilution was used for blotting) against MCV T antigens were generated against MCV large T antigen residues 1–260 and produced as a glutathione *S*-transferase fusion protein in bacteria[50].

MudPIT. MudPIT was performed with MKL-1 and WaGa suspension cells harvested in EBC lysis buffer. Clarified cell extract (100–300 mg) was incubated overnight at 4 °C with 20 μg antibodies cross-linked to 30 mg protein G agarose beads by dimethyl pimelimidate. Beads were washed with high-salt wash buffer five times, then eluted with 0.2 M glycine (pH 3) and neutralized with 1 M Tris (pH 8.0). Proteins were precipitated with 1/5 trichloroacetic acid overnight at 4 °C, washed with cold acetone twice and analysed by MudPIT as described[22]. The endoproteinase Lys-C and trypsin digested peptides were loaded on a split-triple-phase fused-silica microcapillary column and placed in-line with a linear ion trap mass spectrometer (LTQ; Thermo Fisher Scientific) coupled with a Quaternary Agilent 1100 Series high-performance liquid chromatography system. A fully automated ten-step chromatography run was carried out. Each full mass spectrometry scan (400–1,600 *m/z*) was followed by five data-dependent tandem mass spectrometry (MS/MS) scans.

The MS/MS dataset was searched using ProLuCID (version 1.3.3)[51] against a database consisting of 36,628 non-redundant *Homo sapiens* proteins (downloaded from the National Center for Biotechnology Information RefSeq database on 10 June 2016), 193 usual contaminants and (to estimate false discovery rates (FDRs)) 36,821 randomized amino acid sequences derived from each non-redundant protein entry. To account for alkylation by 2-chloroacetamide (CAM), a carbamidomethylation mass shift (+57 Da) was added statically to the cysteine residues. To account for the oxidation of methionine to methionine sulfoxide, a 16 Da mass shift was searched as a differential modification. Peptide/spectrum matches were sorted and selected to an FDR of <5% at the peptide and protein levels, using DTASelect in combination with swallow (an in-house software package). Original mass spectrometry data can be accessed from the ProteomeXchange Consortium (PXD012516) and MassIVE (MSV000083364), and from the Stowers Original Data Repository (at LIBPB-1380).

ChIP-qPCR and RT-qPCR. The ChIP method was modified from protocols described by Schmidt et al.[52]. MKL-1 and IMR90 cells were cross-linked using dual cross-linking with disuccinimidyl glutarate and formaldehyde. After cross-linking, the cells were lysed using SimpleChIP buffers A and B (Cell Signaling Technology), and the DNA was processed with micrococcal nuclease (New England Biolabs) for 30 min at 37 °C followed by sonication for 20 s pulses five times at 4 °C. For RT-qPCR, total RNA was purified using an RNeasy Plus Mini Kit (Qiagen), and complementary DNA was synthesized using the High Capacity cDNA Reverse Transcription kit (Applied Biosystems). Quantitative PCR was performed using Brilliant III Ultra-Fast SYBR Green qPCR Master Mix (Agilent Technologies). The primer information can be found in Supplementary Table 28.

Genome-wide CRISPR screening. CRISPR lentiviral libraries H1 and H2 each contain 92,817 pooled sgRNA sequences targeting 18,493 human genes. CRISPR screening was performed by following a previous protocol[53]. Briefly, 2×10^8 MKL-1 cells were transduced with H1 and H2 CRISPR libraries separately at a multiplicity of infection of 0.3 to ensure single sgRNA incorporation per cell. After 6 d of 1 μg ml^{-1} puromycin selection, surviving cells from each sgRNA library transduction were split into three groups, 3×10^7 cells were saved as initial state controls, the remaining two-thirds were divided into two groups and they were treated with either DMSO or an IC_{30} of GSK-LSD1 (1.4 nM; Sigma–Aldrich). These two groups were cultured for 20 d, with at least 3×10^7 cells maintained and used as final-state samples. Genomic DNA was extracted and 200 μg from each sample was used to PCR amplify integrated sgRNA sequences and to generate four libraries for next-generation sequencing. Some 50 million reads were obtained for each sequencing library. Copy numbers of every 50-kb segment of the MKL-1 genome were called from the input of ChIP-Seq experiments using QDNAseq software[5]. Segmented copy numbers were converted to copy numbers per gene based on gene coordinates. MAGeCK and MAGeCKFlute pipelines were used to assess the data quality, correct the copy number variation effect and identify statistically significant targets[46,53].

Omni-ATAC-Seq. Two independent replicates of 70,000 MKL-1 MCC cells were harvested for ATAC-Seq after treatment with 0.1 μM GSK-LSD1, 0.1 μM dBRD9 or both for 3 d. The cells were washed with PBS twice to achieve >85% viable cells in pellets. The ATAC-Seq protocol was modified from Corces et al.[54]. The transpose reaction was performed using TDE1 Tn5 transposase (15027865; Illumina) and TD buffer (15027866; Illumina). The reactions were cleaned up using a MinElute PCR Purification Kit (28004; Qiagen) and amplified using NEBNext High-Fidelity 2× PCR Master Mix (M0541S; New England Biolabs) for a total of seven cycles. The libraries were cleaned up using the MinElute PCR Purification Kit and additionally with AMPure XP beads (Beckman Coulter) to remove primer dimers and large fragments.

To sequence the libraries, a NextSeq 550 system (Illumina) was used at the Center for Cancer Computational Biology and Molecular Biology Core Facilities following the manufacturer's paired-end sequencing protocol. For analysis, the adapters were removed using NGmerge[55], and the reads were mapped to the hg38 reference using Bowtie 2 (ref. [56]) and sorted by SAMtools[57]. ATAC-Seq peaks were merged, annotated and visualized using BEDtools[43] and the ChIPseeker[58], ChIPpeakAnno[27] and DiffBind[59] R packages and Integrative Genomics Viewer (Broad Institute)[44].

Pathway analysis of gene expression. RNA-Seq of MKL-1 and WaGa MCC cell lines expressing three independent shRNA sequences targeting EP400, an shRNA and a microRNA targeting MYCL, or an shRNA targeting MCV small T antigen, was reported by Cheng et al.[5]. Differentially induced genes for each condition were selected with a fold-change cut-off of 1.5 and FDR cut-off of 0.1. The pathway analysis was performed using the clusterProfiler R package[48] and the differentially enriched GOTERM biological process pathway terms were called using an FDR cut-off of 0.05.

ChIP-Seq analysis. For ChIP-Seq, 30 ng DNA from the ChIP experiments or input DNA were prepared for sequencing with a NEBNext ChIP-Seq Library Prep Reagent Set for Illumina (New England Biolabs). Amplified libraries were cleaned up using AMPure XP beads (Beckman Coulter) and checked on a Bioanalyzer (Agilent) to confirm a narrow distribution with a peak size of around 275 bp. Diluted libraries were used for 50 cycles of single-end sequencing on HiSeq 2000 or NextSeq 550 systems (Illumina) at the Center for Cancer Computational Biology and Molecular Biology Core Facilities following the manufacturer's protocol. ChIP-Seq mapping was performed using Bowtie 2 against human genome version hg19. allowing only uniquely mapping reads[56]. Peak calling was done using MACS2 on either single replicate mapped files or replicates merged as mapped BAM files[60]. ChIP-Seq peaks were merged, annotated and visualized using BEDtools[43] and the ChIPseeker[58], ChIPpeakAnno[27] and DiffBind[59] R packages and Integrative Genomics Viewer (Broad Institute)[44].

RNA-Seq analysis and target prediction. Merkel cell lines in the exponential growth phase were treated in triplicate with 1 μM CPI-242 (MKL-2, WaGa, BroLi, PeTa and UISO) or GSK-LSD1 (MKL-1 and MS-1) for 24 or 72 h. Total RNA was purified using an RNeasy Plus Mini Kit (Qiagen). mRNA was isolated with a NEBNext Poly(A) mRNA Magnetic Isolation Module (New England Biolabs). Sequencing libraries were prepared with an Illumina TruSeq RNA Sample Preparation Kit (version 2; Illumina) or NEBNext mRNA Library Prep Master Mix Set for Illumina (New England Biolabs) and passed Qubit, Bioanalyzer and qPCR quality control analyses. A total of 50 cycles of single-end sequencing were performed on HiSeq 2000 or NextSeq 550 systems. Reads were mapped to the Hg19 genome using STAR[61]. HTSeq was used to create a count file containing gene names[62]. The R package DESeq2 was used to normalize counts, determine differential gene expression and visualize the results[42]. Gene Ontology term enrichment was performed using DAVID Bioinformatics Resources (National Institutes of Health)[45] and the terms were summarized and visualized using REVIGO[63]. Heatmaps depict the average standardized expression profiles and were created using the Heatmap function in the R package ComplexHeatmap[64]. The volcano plot showing global gene expression changes was made with the R package Enhancedvolcano[65]. ChIP-Seq data were integrated with individual differential expression data from RNA-Seq using the Binding and Expression Target Analysis software package, which infers activating or repressive functions of transcription factors and predicts the target genes based on the rank product of binding potential and differential expression[26].

Xenograft efficacy study. Female 7-week-old NSG mice (The Jackson Laboratory) were implanted with 10×10^6 MKL-1 or WaGa MCC cells, with 50% Matrigel, subcutaneously. When the tumours reached the size of 150 mm^3, a group of eight mice for each cell line model were randomized and treated once weekly with vehicle or CPI-242 (Constellation Pharmaceuticals; 40 mg kg^{-1} of 0.5% methylcellulose (400 cP) in 50 mM phosphate buffer (pH 6.8)) by oral gavage. The study was terminated when the tumour volume exceeded the maximum permissible size of 2,000 mm^3 in the vehicle control group. The DFCI Institutional Animal Care and Use Committee approved this study. The study was compliant with all of the relevant ethical regulations regarding animal research.

Multiplexed isobaric tag-based profiling of proteins. Quantitative multiplexed proteomics was performed as described previously[66]. Cells were lysed in 8 M Urea (Sigma–Aldrich) containing a cocktail of phosphatase and protease inhibitors (Roche) buffered with HEPES (Sigma–Aldrich) to a pH of 8.5. Xenograft tissues were placed in the same urea lysis buffer and homogenized with a handheld tissue drill. All lysates were homogenized by passing the lysate through a 22-gauge needle before passage through a 25-gauge needle followed by sedimentation by centrifugation at 21,000*g* for 15 min. The supernatant was transferred to a new tube and the protein concentration was determined by bicinchoninic acid assay (Thermo Fisher Scientific). The proteins were then reduced and alkylated to block reactive cysteine groups, then chloroform-methanol precipitated. Proteins were resuspended in 200 mM EPPS buffer (pH 8.5), digested with Lys-C (Wako) overnight at room temperature and subsequently digested with sequencing-grade trypsin (Promega) for 6 h at 37 °C. Digests were then labelled with a TMT10 reagent for 90 min at room temperature and then quenched with hydroxylamine. The quenched reaction was then combined at a 1:1:1:1:1:1:1:1:1:1 mass ratio, flash frozen and dried down in a vacuum centrifuge. The sample was resuspended in 1% formic acid, desalted using C18 solid-phase extraction (Sep-Pak; Waters) and dried down in a vacuum centrifuge before resuspension in 10 mM ammonium bicarbonate and 5% acetonitrile for off-line basic pH reversed-phase fractionation. Off-line basic pH reversed-phase high-performance liquid chromatography was performed on an Agilent 1260 pump. A gradient of 13–37% acetonitrile in 10 mM ammonium bicarbonate was used over 50 min. Whole-proteome fractions were collected in a 96-well plate and combined into 24 fractions, of which only non-adjacent samples were analysed, as described previously[66]. The pooled tandem mass tag (TMT)-labelled sample and the phosphopeptide-enriched sample were each separated into 96 fractions by the instrument. For each fractionation experiment, fractions were collected in a 96-well plate and combined into 24 fractions as described previously. The 24 fractions were acidified to 1% formic acid and dried down in a vacuum centrifuge. Dried-down fractions were resuspended in 5% acetonitrile and 5% formic acid for liquid chromatography MS/MS (LC-MS/MS) analysis.

Data for all quantitative TMT LC-MS/MS experiments were collected on an Orbitrap Fusion mass spectrometer (Thermo Fisher Scientific) with liquid chromatography separation performed on an attached Proxeon EASY-nLC 1200 liquid chromatography pump (Thermo Fisher Scientific). The LC-MS/MS method was modified from a previous study. A 100-μm inner-diameter microcapillary column packed with 35 cm of Accucore C18 resin (2.6 μm; 150 Å; Thermo Fisher Scientific) was used to separate the peptides. Approximately 2 μg of peptide was loaded onto the column for analysis. A 150-min gradient of 6–25% acetonitrile in 0.125% formic acid was used at a flow rate of ~450 nl min^{-1} to separate the peptides from the pooled TMT-labelled samples (MS1 spectra; Orbitrap resolution: 120,000; mass range: 350–1,400 m/z; automatic gain control (AGC) target: 5×10^5; maximum injection time: 100 ms). We then used a Top10 method to select precursors for further downstream analysis. MS2 spectra were collected after collision-induced dissociation (AGC target: 2×10^4; normalized collision energy: 35%; maximum injection time: 120 ms; isolation window: 0.7 Th). MS2 analysis was performed in the ion trap. We performed an MS3 analysis for each MS2 scan acquired by isolating multiple MS2 fragment ions that were used as precursors for the MS3 analysis with a multi-notch isolation waveform. We detected the MS3 analysis in the Orbitrap (resolution: 50,000) after high-energy collision-induced dissociation (normalized collision energy: 65%; AGC target: 2.5×10^5; maximum injection time: 150 ms; isolation window: 1.3 Th).

TMT LC-MS/MS data analysis. Spectra acquired from the LC-MS/MS experiments for the TMT experiments were processed using a SEQUEST-based software pipeline. First, a modified version of ReAdW.exe converted the spectra to the mzXML format. These files were then searched against a database that contained the human proteome (UniProt database organism ID: 9606; downloaded 26 May 2018) and MCV small and large T antigens concatenated to a database of all protein sequences reversed. For the xenograft studies, a mouse proteome was appended to the database (UniProt database organism ID: 10090; downloaded 26 May 2018) before reversal and concatenation. Mouse and human proteins are distinguished by their peptide identifications. The SEQUEST search engine takes care of assignments of peptides to mass spectra[67]. A precursor ion tolerance of 50 p.p.m. and a production tolerance of 0.9 Da were used as search parameters. Static modifications for TMT tags (+229.163 Da) on lysine residues and the peptide's amino terminus, and carbamidomethylation (+57.021 Da) on cysteine residues, were used in conjunction with a variable modification for oxidation (+15.995 Da) on methionine. Peptide–spectrum matches were then filtered using linear discriminant analysis to an FDR of 1%, as described previously[68]. XCorr, ΔCn, missed cleavages, peptide length, charge state and precursor mass accuracy were used as parameters for the linear discriminant analysis. The FDR was estimated using the target-decoy method. Peptides were identified and collapsed using principles of parsimony to a final protein-level FDR of 1%. For quantitation, we extracted the signal-to-noise ratio of the closest matching centroid to the expected mass of the TMT reporter ion for each TMT channel from MS3 scans triggered by MS2 scans. MS3 spectra were filtered for a minimum TMT reporter ion sum signal-to-noise ratio of 200 and an isolation specificity of at least 0.5. Protein-level fold-changes were calculated by comparing the sum signal-to-noise ratios for all observed peptides of a given protein. Proteins were ranked by nominal P values obtained from Tukey's honest significance test performed post hoc on peptide-level linear models for each protein. These P values were adjusted for multiple testing by employing the Benjamini–Hochberg method at a condition pairwise level to adjust FDRs. Pattern matching was performed by converting a desired protein expression pattern into a vector of eight values, corresponding to the TMT channels used in the experiment, with each value taking a number between 0 (no expression) and 100 (full expression). This vector was compared with a vector of the scaled TMT values for each protein by calculating a cosine similarity value, with values closer to 1 indicating more similarity.

Statistics and reproducibility. To ensure reproducibility, all of the western blotting experiments were performed at least three times and only the representative data with similar results are reported in the study. Statistical analysis details can be found in the figure captions and Methods.

Reporting Summary. Further information on research design is available in the Nature Research Reporting Summary linked to this article.

Data availability

ATAC-Seq, ChIP-Seq and RNA-Seq data that support the findings of this study have been deposited in the Gene Expression Omnibus under accession codes GSE124856, GSE124857, GSE124861, GSE124864 and GSE140505. The mass spectrometry data are available at the ProteomeXchange Consortium under accession code PXD012516. All other data supporting the findings and computer codes implemented in this study are available from the corresponding author on reasonable request. Source data for Figs. 1–8 and Extended Data Figs. 1–3 and 7 are presented with the paper.

References

49. Carey, M. F., Peterson, C. L. & Smale, S. T. Dignam and Roeder nuclear extract preparation. *Cold Spring Harb. Protoc.* **2009**, pdb.prot5330 (2009).
50. Cheng, J., Rozenblatt-Rosen, O., Paulson, K. G., Nghiem, P. & DeCaprio, J. A. Merkel cell polyomavirus large T antigen has growth-promoting and inhibitory activities. *J. Virol.* **87**, 6118–6126 (2013).
51. Xu, T. et al. ProLuCID: an improved SEQUEST-like algorithm with enhanced sensitivity and specificity. *J. Proteomics* **129**, 16–24 (2015).
52. Schmidt, D. et al. ChIP-Seq: using high-throughput sequencing to discover protein–DNA interactions. *Methods* **48**, 240–248 (2009).
53. Mertins, P. et al. Reproducible workflow for multiplexed deep-scale proteome and phosphoproteome analysis of tumor tissues by liquid chromatography–mass spectrometry. *Nat. Protoc.* **13**, 1632–1661 (2018).
54. Corces, M. R. et al. An improved ATAC-Seq protocol reduces background and enables interrogation of frozen tissues. *Nat. Methods* **14**, 959–962 (2017).
55. Gaspar, J. M. NGmerge: merging paired-end reads via novel empirically-derived models of sequencing errors. *BMC Bioinformatics* **19**, 536 (2018).
56. Langmead, B. & Salzberg, S. L. Fast gapped-read alignment with Bowtie 2. *Nat. Methods* **9**, 357–359 (2012).
57. Li, H. et al. The Sequence Alignment/Map format and SAMtools. *Bioinformatics* **25**, 2078–2079 (2009).
58. Yu, G., Wang, L.-G. G. & He, Q.-Y. Y. ChIPseeker: an R/Bioconductor package for ChIP peak annotation, comparison and visualization. *Bioinformatics* **31**, 2382–2383 (2015).
59. Ross-Innes, C. S. et al. Differential oestrogen receptor binding is associated with clinical outcome in breast cancer. *Nature* **481**, 389–393 (2012).
60. Zhang, Y. et al. Model-based analysis of ChIP-Seq (MACS). *Genome Biol.* R137 (2008).
61. Dobin, A. et al. STAR: ultrafast universal RNA-Seq aligner. *Bioinformatics* **29**, 15–21 (2013).
62. Anders, S., Pyl, P. T. & Huber, W. HTSeq—a Python framework to work with high-throughput sequencing data. *Bioinformatics* **31**, 166–169 (2015).
63. Supek, F., Bošnjak, M., Škunca, N. & Šmuc, T. REVIGO summarizes and visualizes long lists of gene ontology terms. *PLoS ONE* **6**, e21800 (2011).
64. Gu, Z., Eils, R. & Schlesner, M. Complex heatmaps reveal patterns and correlations in multidimensional genomic data. *Bioinformatics* **32**, 2847–2849 (2016).
65. Blighe, K., Rana, S. & Lewis, M. EnhancedVolcano: Publication-ready volcano plots with enhanced colouring and labeling. R package version 1.4.0 (2019).
66. Navarrete-Perea, J., Yu, Q., Gygi, S. P. & Paulo, J. A. Streamlined tandem mass tag (SL-TMT) protocol: an efficient strategy for quantitative (phospho) proteome profiling using tandem mass tag-synchronous precursor selection-MS3. *J. Proteome Res.* **17**, 2226–2236 (2018).
67. Ting, L., Rad, R., Gygi, S. P. & Haas, W. MS3 eliminates ratio distortion in isobaric multiplexed quantitative proteomics. *Nat. Methods* **8**, 937–940 (2011).
68. Elias, J. E. & Gygi, S. P. Target-decoy search strategy for increased confidence in large-scale protein identifications by mass spectrometry. *Nat. Methods* **4**, 207–214 (2007).

Acknowledgements

We are grateful to C. Kadoch (DFCI) and members of the Kadoch laboratory for helpful discussions relating to mSWI/SNF and specifically ncBAF complex biology and experimental approaches, Y. Shi (Boston Children's Hospital) for providing valuable insights on LSD1, X. S. Liu (DFCI) for consultation about the CRISPR–Cas9 screen analysis, and S. Gygi (Harvard Medical School), J. Qi (DFCI) and M. Brown (DFCI) for sharing reagents and equipment. This work was supported in part by the US Public Health Service (grant F31CA213464 to D.E.P. and grants R35CA232128, R01CA63113, R01CA173023 and P01CA203655 to J.A.D.). J.A.D. received research funding from Constellation Pharmaceuticals. S.K.S., L.F. and M.P.W. were supported by the Stowers Institute for Medical Research. J.A.P. was supported by NIH NIGMS grant R01GM132129.

Author contributions

D.E.P. and J.A.D. conceived of the study. D.E.P. and J.A.D. developed the methodology. D.E.P., M.Y.L. and L.F. developed the software. D.E.P. and J.C. validated the results. D.E.P., M.Y.L., L.F., C.C., J.P.M. and P.C.G. performed the formal analysis. D.E.P., J.C., J.P.M., M.Y.L., S.K.S. and M.L.T. performed the investigation. J.A.P., P.C.G., M.P.W., P.T. and J.A.D. provided resources. D.E.P. and J.A.D. wrote the original draft of the manuscript. D.E.P., J.C., J.P.M., M.Y.L., L.F. and J.A.D. reviewed and edited the manuscript. D.E.P. and M.Y.L. visualized the results. P.T., P.C.G., M.P.W. and J.A.D. supervised the study. P.T. and J.A.D. acquired funding.

Competing interests

J.P.M. and P.T. are employees of Constellation Pharmaceuticals. J.A.D. received research funding from Constellation Pharmaceuticals. J.A.D. has served as a consultant to Merck & Co. and EMD Serono.

Additional information

Extended data is available for this paper at https://doi.org/10.1038/s41556-020-0503-2.

Supplementary information is available for this paper at https://doi.org/10.1038/s41556-020-0503-2.

Correspondence and requests for materials should be addressed to J.A.D.

Reprints and permissions information is available at www.nature.com/reprints.

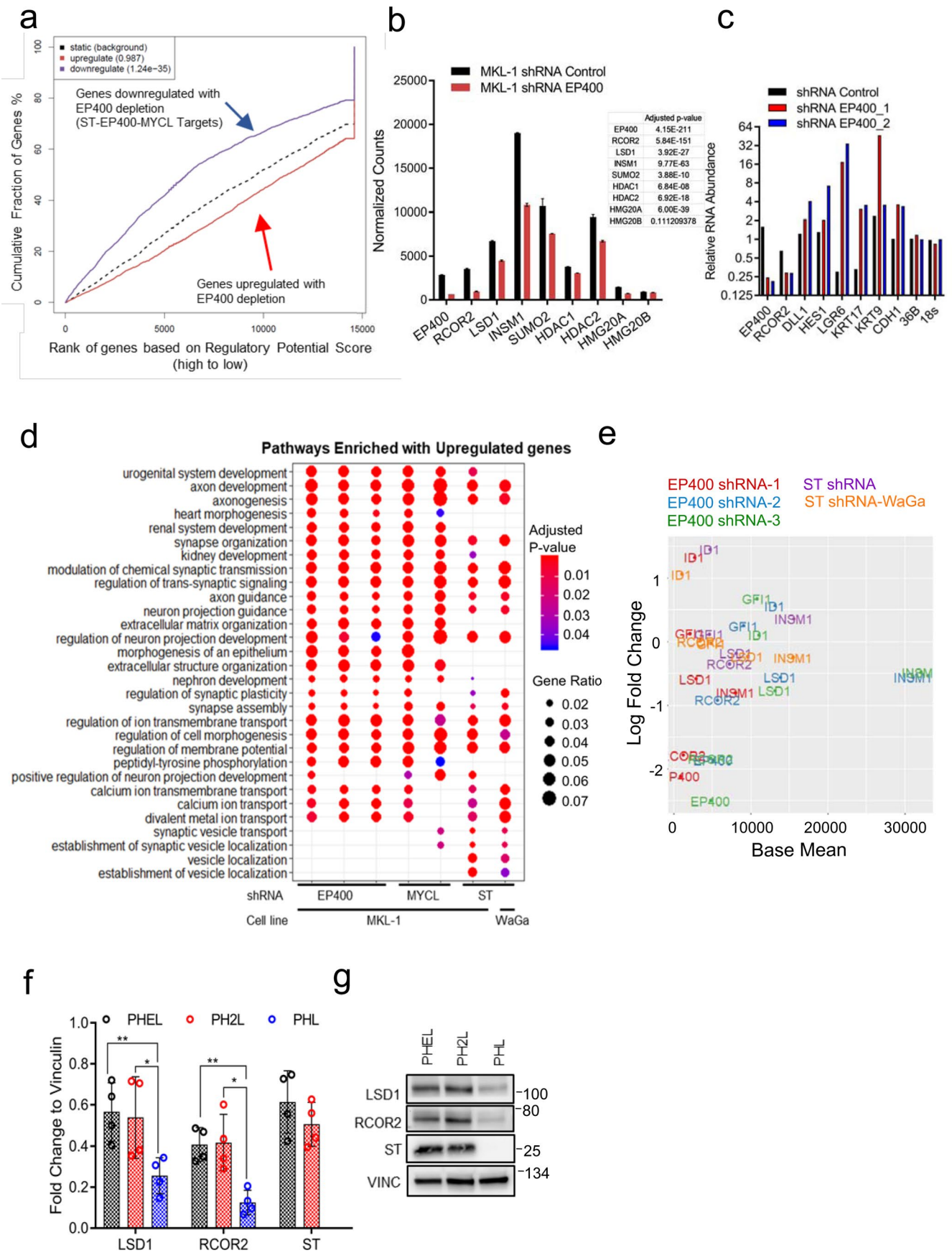

Extended Data Fig. 1 | See next page for caption.

Extended Data Fig. 1 | Merkel small T antigen transactivates LSD1 complex components. a, Integrated ChIP- and RNA-seq analysis of the MCV ST target genes predicts that MCV ST forms an activator complex. **b**, RNA-seq results show that EP400 depletion in MKL-1 leads to a reduction in mRNA levels of RCOR2, LSD1, INSM1, and additional components of the LSD1 complex. DESeq2 normalized counts were plotted. Differentially expressed genes were found by comparing each condition with DESeq2 and p-values were adjusted by Benjamini-Hochberg. **c**, Two independent shRNAs against EP400 decrease levels of EP400 and RCOR2 levels but increase levels of DLL1, HES1, LGR6, KRT17, KRT9, and CDH1 in MKL-1 cells. The RT-qPCR signals were normalized to each uninduced sample and the geomean of 36B (RPLP0) and 18 s rRNA. **d**, Depletion of EP400, MYCL, or MCV ST by shRNA leads to increased levels of genes involved in critical cancer and differentiation pathways in MKL-1 and WaGa MCC cell lines (n = 3 independent biological replicates used in each condition). The enrichment test was performed on hypergeometric distribution and the p-values were adjusted by FDR (Supplementary Tables 1–3). **e**, RNA-seq of MKL-1 cells expressing three independent shRNAs targeting EP400 or ST in MKL-1 and WaGa cells was performed. Mean expression was plotted against log fold change. **f**, The LSD1 and RCOR2 levels were significantly higher in PHEL (+MCV LT and wild-type ST) and PH2L (+MCV LT and the ST mutant E86S-E87S unable to bind the EP400) than in PHL (-MCV T antigens). The fold changes in the western blot signals from four replicate experiments were averaged. Data are shown as mean of n = 4 ± SD; two-sided t-test, *$P < 0.05$; **<0.005. **g**, A representative blot for Extended Data Fig 1g is shown. The experiment was performed four times. See Unprocessed Gels Extended Data Fig. 1.

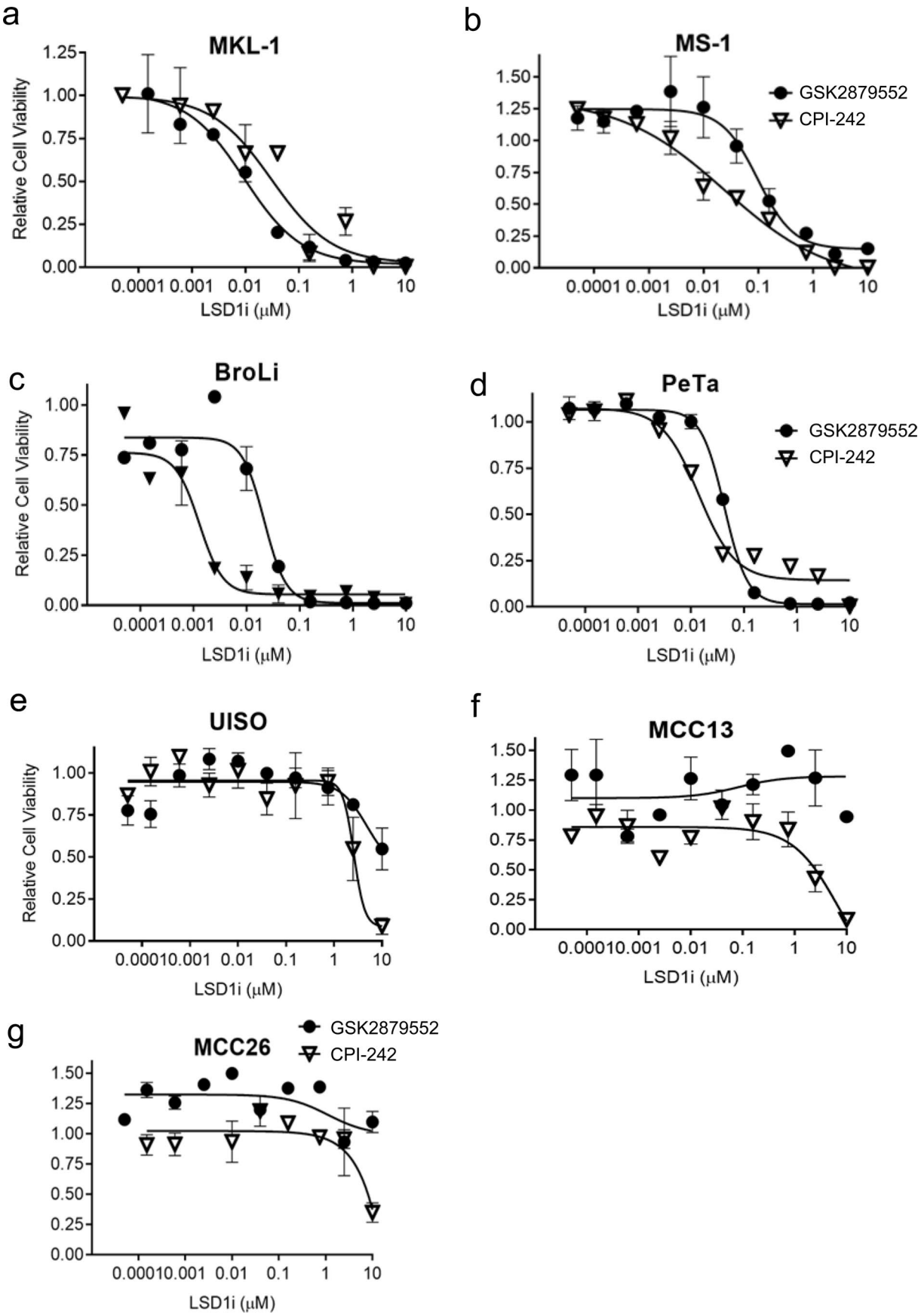

Extended Data Fig. 2 | LSD1 inhibition reduces the growth of virus-positive MCC cell lines. a-**g**, Virus-positive (**a**-**d**), but not virus-negative (**e**-**g**), MCC cell lines are sensitive to two independent LSD1 inhibitors (GSK2879552 and CPI-670242) in a dose-dependent manner. Relative viability was measured at 12 days of treatment by the CellTiter-Glo assay. Data are shown as mean ± SD and reflect three biological replicates.

a

	SMAD9	SMARCA1
	Adjusted p-value	Adjusted p-value
MKL-1	4.29088E-06	1.85023E-08
MKL-2	4.72518E-05	3.73462E-06
MS-1	4.15311E-06	1.12853E-05
WaGa	4.35588E-07	2.20882E-06
PeTa	4.35588E-07	3.28888E-06
BroLi	0.001144988	3.46186E-06
UISO	0.075409163	0.051759784

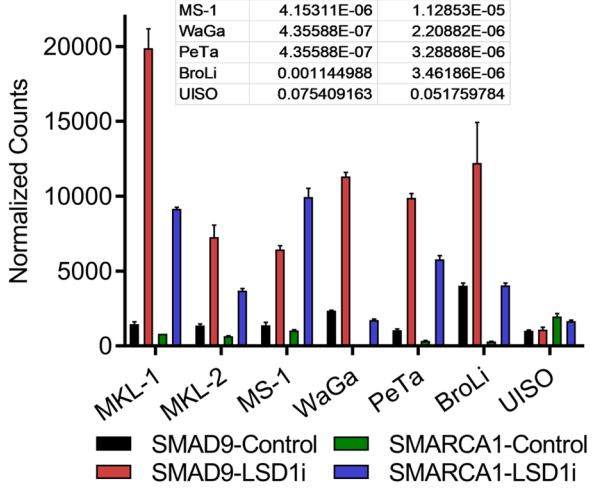

b

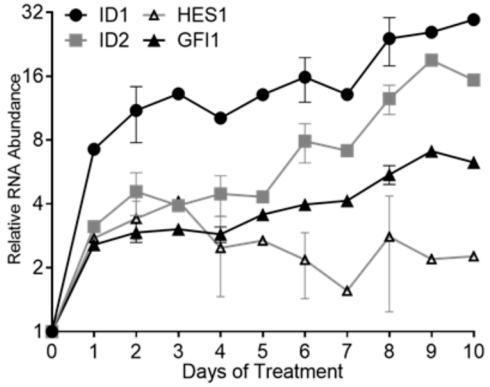

c

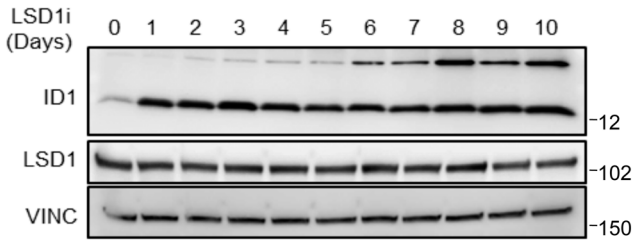

d

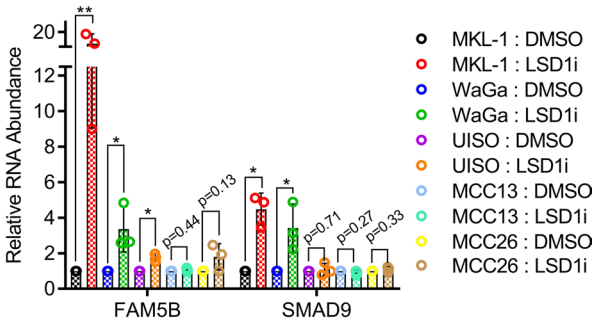

e

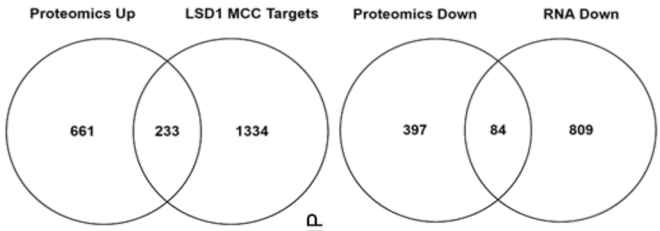

f

Category: Term	-log10(q-value, Bonferroni)
CC: neuron projection	4.605505611
CC: cell projection	4.624575568
CC: synapse	3.090355529
CC: Golgi apparatus	2.48680985
CC: nucleoplasm	2.320839667
BP: neuron differentiation	2.414937284
BP: cell projection morphogenesis	1.715266074
BP: axonogenesis	1.7711349
BP: neuron projection development	1.652644987
BP: protein kinase cascade	1.376181263

g

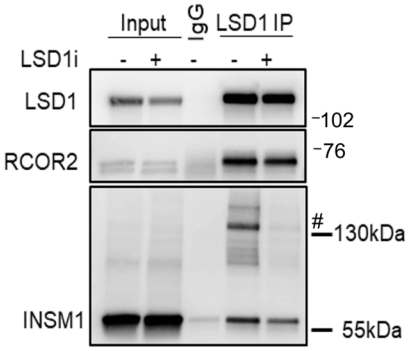

h

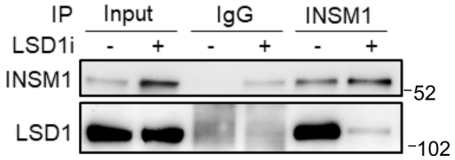

i

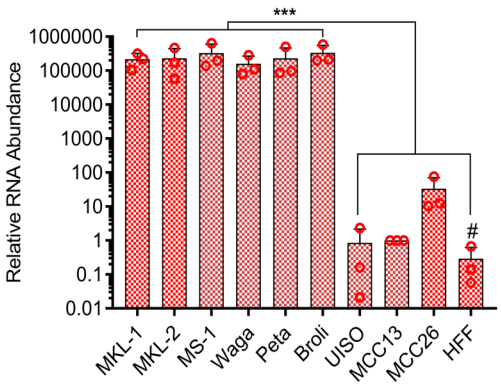

Extended Data Fig. 3 | See next page for caption.

Extended Data Fig. 3 | Integrative ChIP-seq and RNA-seq LSD1 targetome analysis reveal that LSD1 regulates neuronal differentiation pathways in MCC. a, Differential gene expression analysis was performed using DESeq2 and p-values were adjusted by Benjamini-Hochberg. **b**, **c**, RT-qPCR (**b**) and western blot (**c**) assessment of LSD1 target genes in MKL-1 cells of LSD1 inhibition (GSK-LSD1, 1 μM) in triplicate. For **b**, the signals were normalized to untreated samples and RPLP0 in each sample. See Unprocessed Gels Extended Data Fig. 3. **d**, Cells were treated with GSK-LSD1 (0.1 μM) for three days. Data are shown as mean of n = 3 ± SD; two-sided t-test, *P < 0.05; **<0.005. **e**, Multiplexed Isobaric Tag-Based Profiling of MKL-1 treated with GSK-LSD1 for eight days displays global changes in the proteome. The Venn diagrams show the numbers of genes identified in the RNA- and ChIP-seq-based targetome analysis (Fig. 3; LSD1 MCC targets: upregulated following LSD1i with LSD1 ChIP peaks; RNA down: downregulated following LSD1i) and the proteomics experiment (Supplementary Tables 5 and 11; Proteomics up: upregulated following LSD1i; Proteomics down: downregulated following LSD1i). **f**, The targetome analysis was performed by integrating ChIP-seq of LSD1 and RNA-seq of the virus-positive MCC cell lines in three independent biological replicates (Supplementary Table 5). Selected GOTERM biological processes (BP) and Cell compartments (CC) –log10 of Bonferroni adjusted p-values are shown. **g**, The LSD1 IP, followed by western blotting, indicates that LSD1 has reduced binding to INSM1 following LSD1 inhibition. The experiment was performed three times. # non-specific band. See Unprocessed Gels Extended Data Fig. 3. **h**, IP-western blotting shows INSM1 reduced interaction with LSD1. MKL-1 cells were treated with GSK-LSD1 (0.1 μM) for three days and processed for IP. The experiment was performed at least three times. See Unprocessed Gels Extended Data Fig. 3. **i**, RT-qPCR of MCC lines and primary human cells (HFF) were performed in triplicate[60]. Data are shown as mean of n = 3 ± SD; two-sided t-test, ***P < 0.0005. # - below detection level.

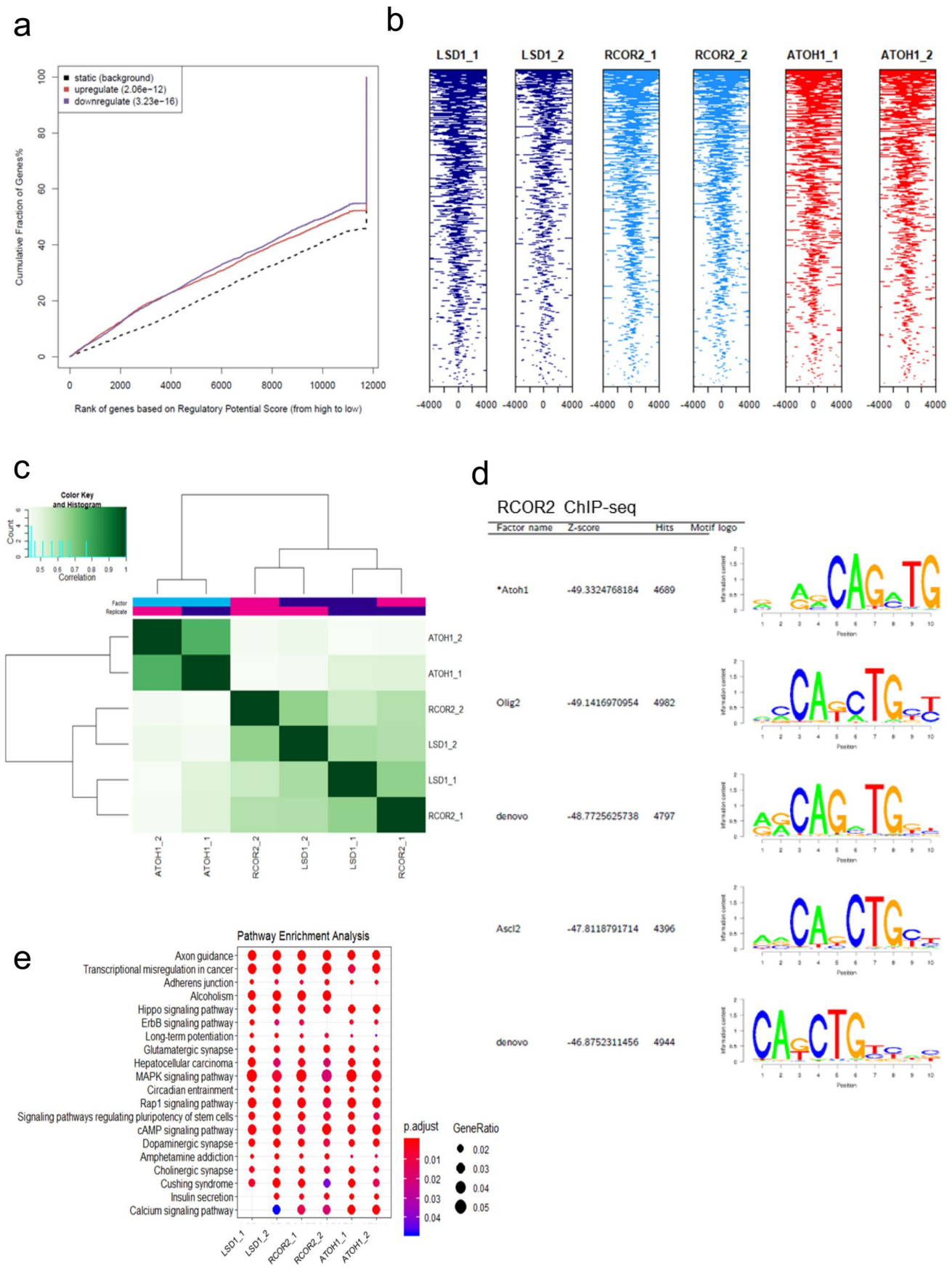

Extended Data Fig. 4 | See next page for caption.

Extended Data Fig. 4 | ChIP-seq of LSD1, RCOR2, and ATOH1 indicates shared DNA occupancy. a, Integrated ChIP- and RNA-seq analysis[35] reveals that genes perturbed by LSD1 inhibition are direct LSD1 targets. **b**, Tag heat maps of two replicates of LSD1 (LSD1_1 and LSD1_2), RCOR2 (RCOR2_1 and RCOR2_2), and ATOH1 (ATOH1_1 and ATOH1_2) ChIP-seq show that the factors bind to common regions close to the transcription start sites (TSSs +/- 4,000 bp). **c**, The heatmap displays correlations among LSD1, RCOR2, and ATOH1 ChIP-seq peaks. **d**, The SeqPos motif tool[36] was used to determine the LSD1 binding motifs in MKL-1. The binding motifs of ATOH1, as well as OLIG2 and ASCL2, were enriched in the RCOR2 (RCOR2_1) ChIP-seq. **e**, GOTERM biological process pathway analysis of the two independent replicates of LSD1, RCOR2, and ATOH1 ChIP-seq revealed that the factors regulate genes involved in neuronal functions and developmental signaling. The enrichment test was performed on hypergeometric distribution and the p-values were adjusted by FDR.

a Upregulated proteins: MKL-1

Category: Term	-log10(q-value, Bonferroni)
BP: axonogenesis	6.432973634
BP: cell morphogenesis involved in neuron differentiation	6.21395879
BP: cell adhesion	5.676578833
BP: vesicle-mediated transport	3.038916553
BP: regulation of neuron differentiation	2.59688795
BP: neuron differentiation	2.328217287
BP: cellular respiration	3.324964272
CC: intrinsic to membrane	6.526159578
CC: neuron projection	4.254649091
CC: synapse	3.361603237
CC: respiratory chain	2.071808219
CC: axon	1.819060148

b Downregulated proteins: MKL-1

Category: Term	-log10(q-value, Bonferroni)
BP: cell cycle	16.45429275
BP: M phase	8.374779145
BP: regulation of transcription	4.457239302
BP: response to DNA damage stimulus	3.252160565
CC: chromosome	14.98914479
CC: chromosomal part	11.77174731

c

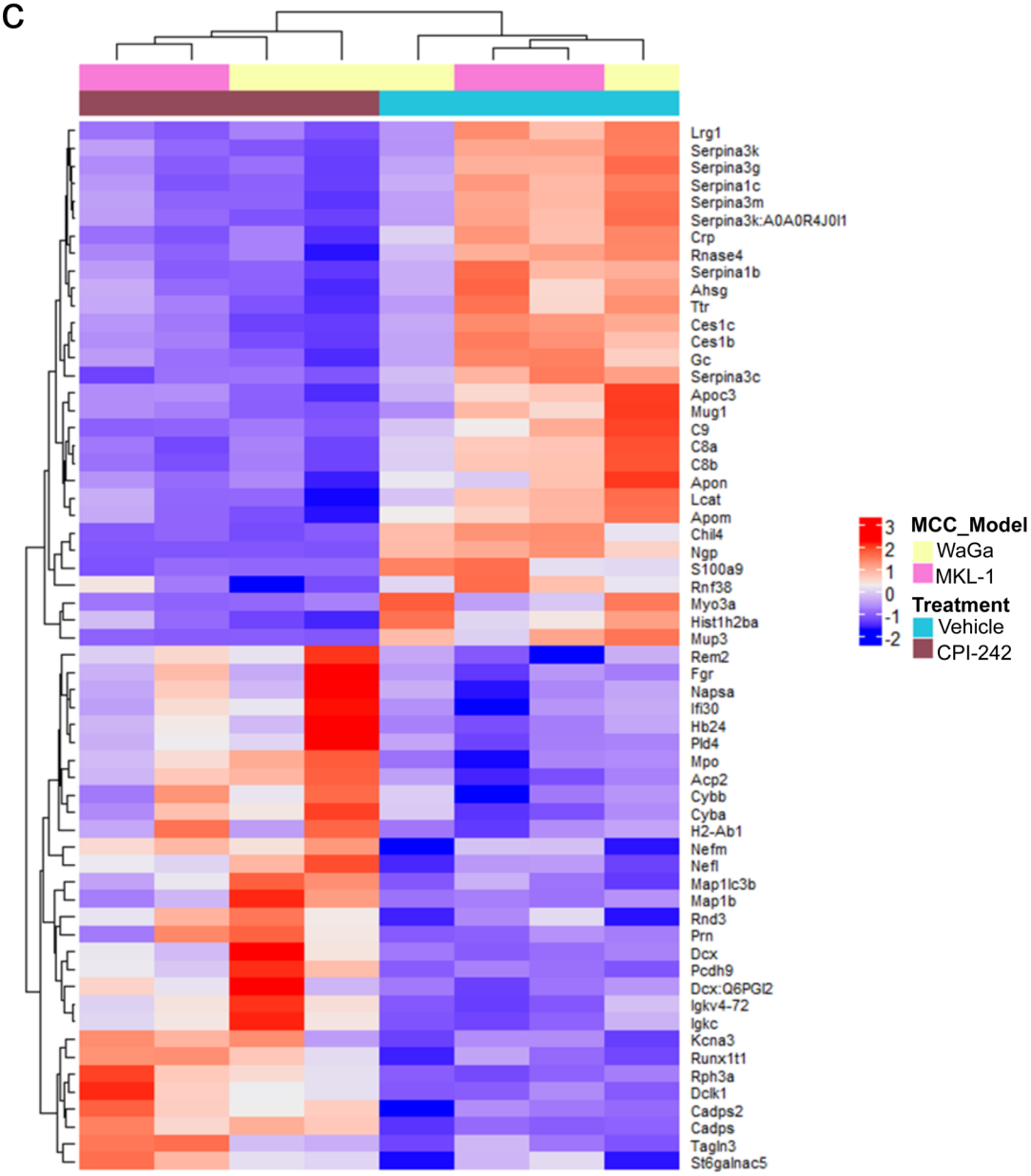

Extended Data Fig. 5 | See next page for caption.

Extended Data Fig. 5 | Multiplexed Isobaric Tag-Based Profiling of MCC-derived xenografts reveals that LSD1 inhibition perturbs neuronal gene expression in human and mouse tissues. a-**b**, The multiplexed Isobaric Tag-Based Profiling of the MKL-1 virus-positive MCC cell line treated with GSK-LSD1 for eight days identified genes that are differentially expressed during LSD1 inhibition. n = 5 independent biological replicates were used for analysis. Selected GOTERM biological process and cellular compartment terms are shown for the upregulated (**a**) and downregulated (**b**) proteins. **c**, Eight mice were injected with MKL-1 or WaGa MCC cells, and when the tumor size reached 150 mm3, two of each four mice for each MCC model were treated with CPI-670242 (40 mg/kg) orally once a week for 22 days. The tumors were harvested for the TMT-10 plex isobaric tag-labeling quantitative mass spectrometry experiment. **c**, The heatmap shows the relative abundance of 30 most upregulated and 30 most downregulated mouse proteins after the treatment.

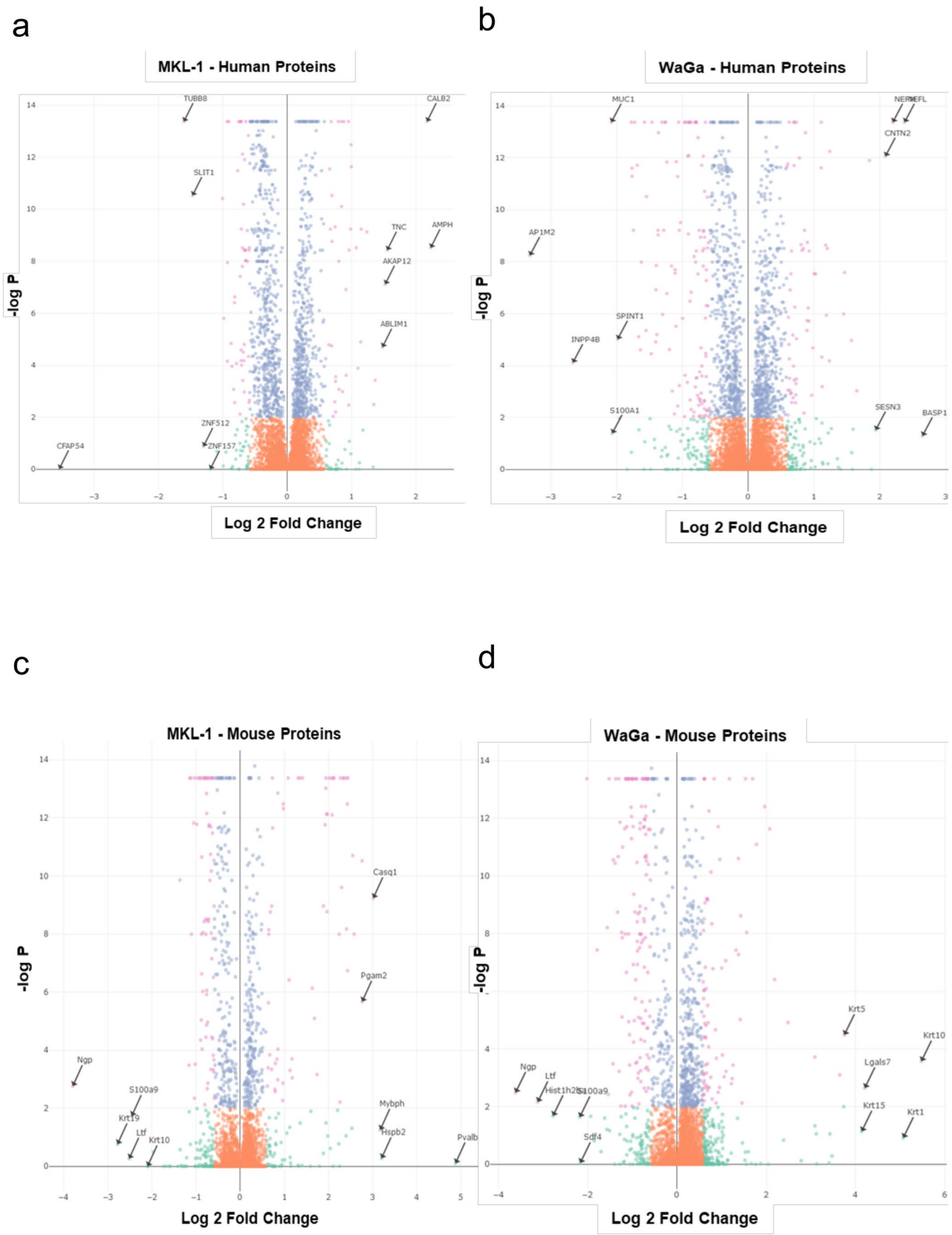

Extended Data Fig. 6 | See next page for caption.

Extended Data Fig. 6 | Multiplexed Isobaric Tag-Based Profiling of MCC-derived xenografts profiles global changes in tumor proteomes. The volcano plots display global protein expression changes of MKL-1 human proteins (**a**), WaGa human proteins (**b**), MKL-1 mouse proteins (**c**), and WaGa mouse proteins (**d**) with or without the LSD1 inhibitor. Tukey's Honest Significance Test was performed post-hoc on-peptide level linear models for each protein and the p-values were adjusted by Benjamini-Hochberg. Each protein is plotted based on its log2 fold change against -log10 of adjusted p-values. The five most upregulated and five most downregulated proteins in each plot are labeled.

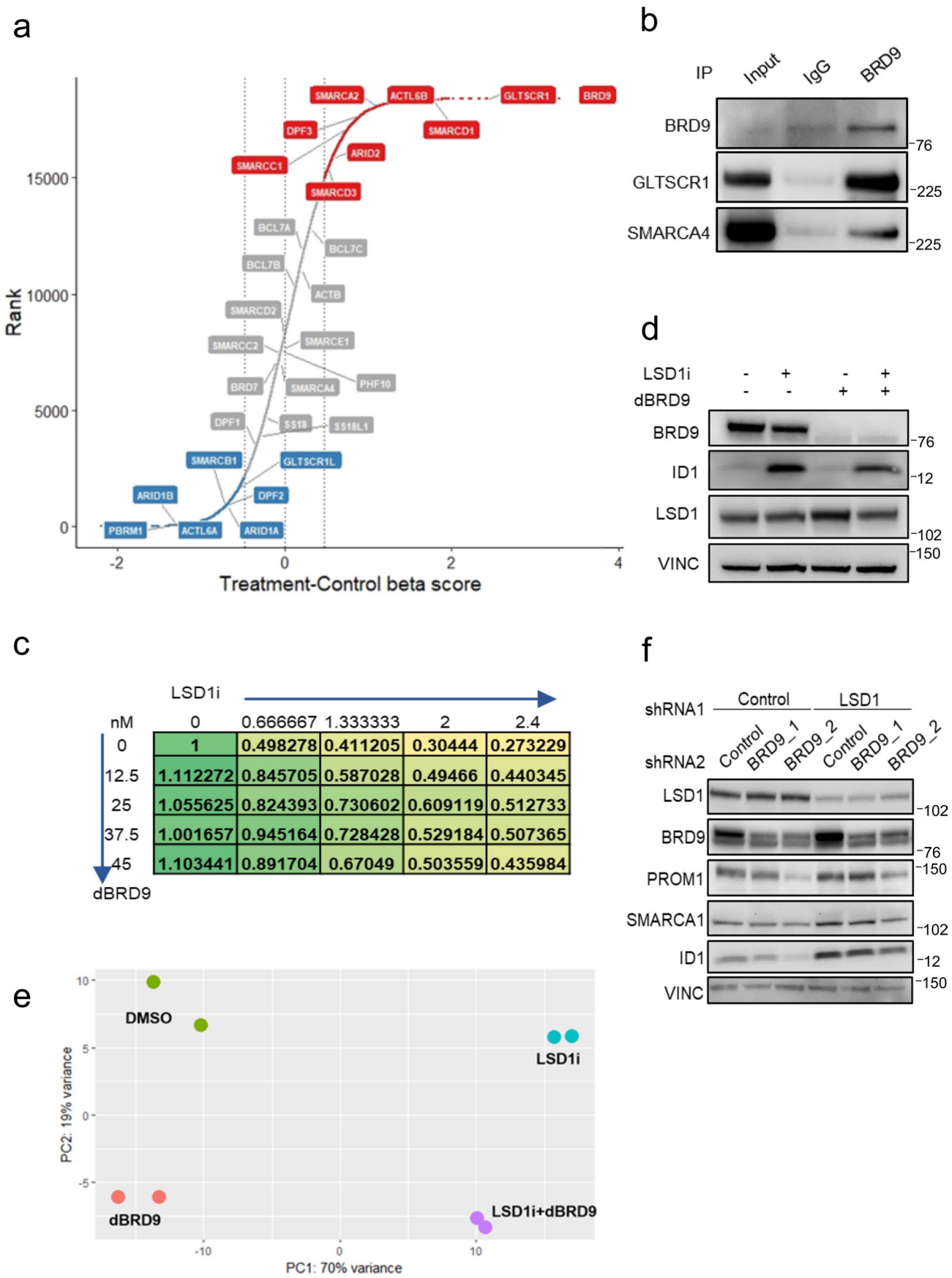

Extended Data Fig. 7 | See next page for caption.

Extended Data Fig. 7 | CRISPR screen shows that LSD1 inhibition creates positive pressure for deleting ncBAF complex components. a, Gene ranks based on the differences of the beta (selection) scores between the treatment (GSK-LSD1, 20 days, IC30–1.5 nM) and control (DMSO 20 days) screens show the positively and negatively selected mSWI/SNF components genes including the ncBAF complex components BRD9, GLTSCR1, SMARCA2, SMARCD1, and SMARCC1 (Supplementary Tables 18–20). The rank list contains all the previously reported mSWI/SNF components. **b**, BRD9 binds to SMARCA4 (BRG1) and GLTSCR1 (BICRA) in MKL-1. IP using a BRD9 antibody followed by western blotting was performed to determine interactions among BRD9, GLTSCR1, and SMARCA4. The experiment was performed at least three times. See Unprocessed Gels Extended Data Fig. 7. **c**, BRD9 degradation restores the loss of cell viability caused by LSD1 inhibition in MCC. MKL-1 cells were treated with varying doses of the dBRD9 and LSD1 inhibitor (GSK-LSD1) for six days. The XTT assay measured relative cell viability. **d**, dBRD9 degrades BRD9 efficiently. MKL-1 cells were treated with GSK-LSD1 (0.1 μM), dBRD9 (0.1 μM), or both for three days and harvested for western blotting. The experiment was performed at least three times. See Unprocessed Gels Extended Data Fig. 7. **e**, The PCA plot shows that the degradation of BRD9 by dBRD9 partially rescues the global gene expression changes caused by LSD1 inhibition. n = 2 independent biological replicates were used for analysis. **f**, BRD9 depletion by shRNAs rescues gene expression changes caused by LSD1 depletion. MKL-1 cells were transduced with an LSD1-targeting shRNA either with a control shRNA or two distinct BRD9-targeting shRNAs for six days and harvested for western blotting. The experiment was performed at least three times. See Unprocessed Gels Extended Data Fig. 7.

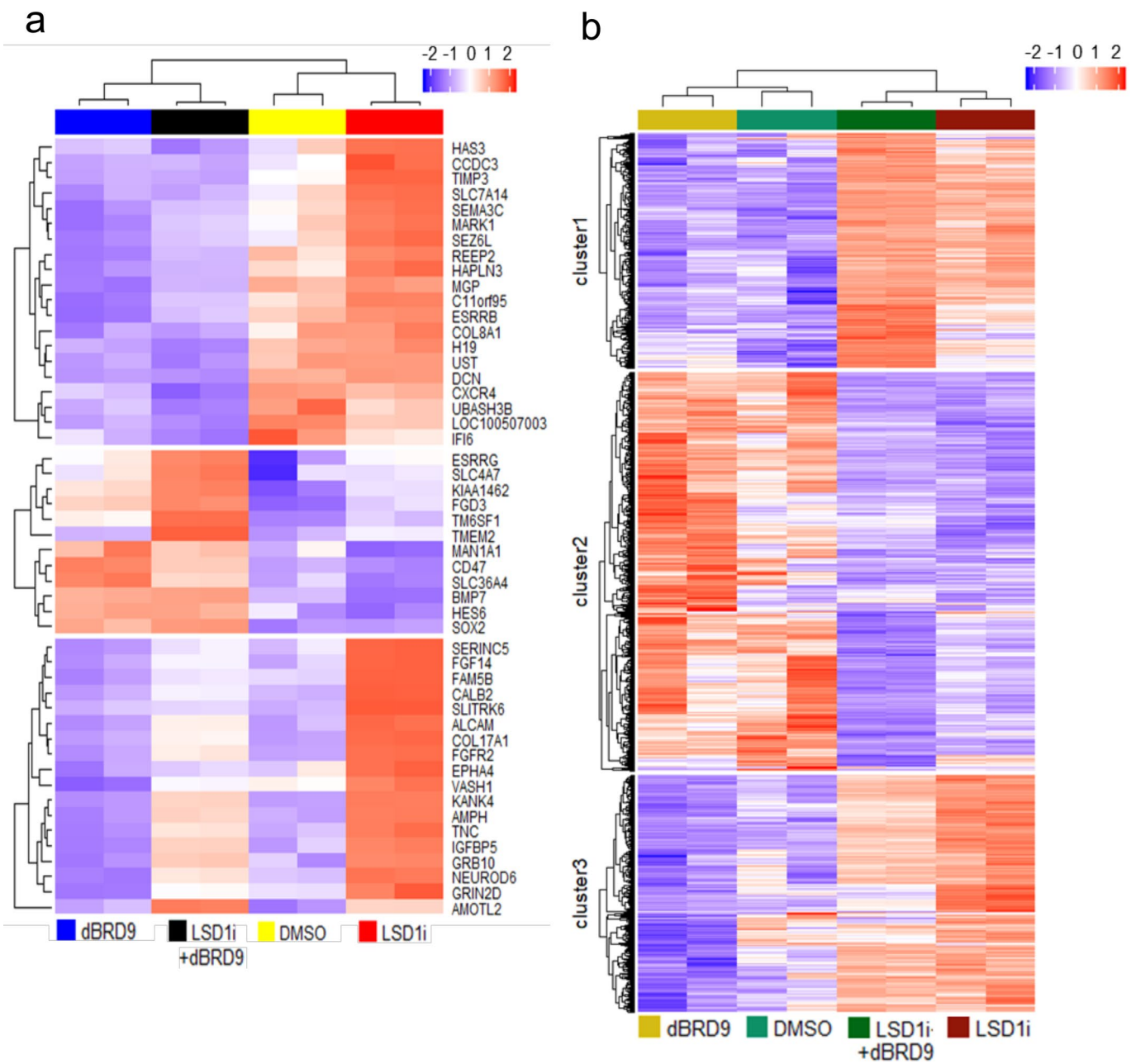

Extended Data Fig. 8 | Heatmaps of gene expression changes following LSD1 and BRD9 inhibition indicate that LSD1 and BRD9 regulate an overlapping set of genes in an antagonistic manner. a, **b**, RNA-seq was performed with n = 2 biologically independent replicates of MKL-1 cells treated with DMSO, GSK-LSD1 (LSD1i, 0.1 μM), dBRD9 (0.1 μM), or both GSK-LSD1 and dBRD9 for six days. **a**, Top 50 most differentially expressed genes between LSD1i and LSD1i + dBRD9 are shown. Differential gene expression analysis was performed using DESeq2 and p-values were adjusted by Benjamini-Hochberg. **b**, All differentially expressed genes (3392 genes; FDR < 0.05) across the conditions are shown.

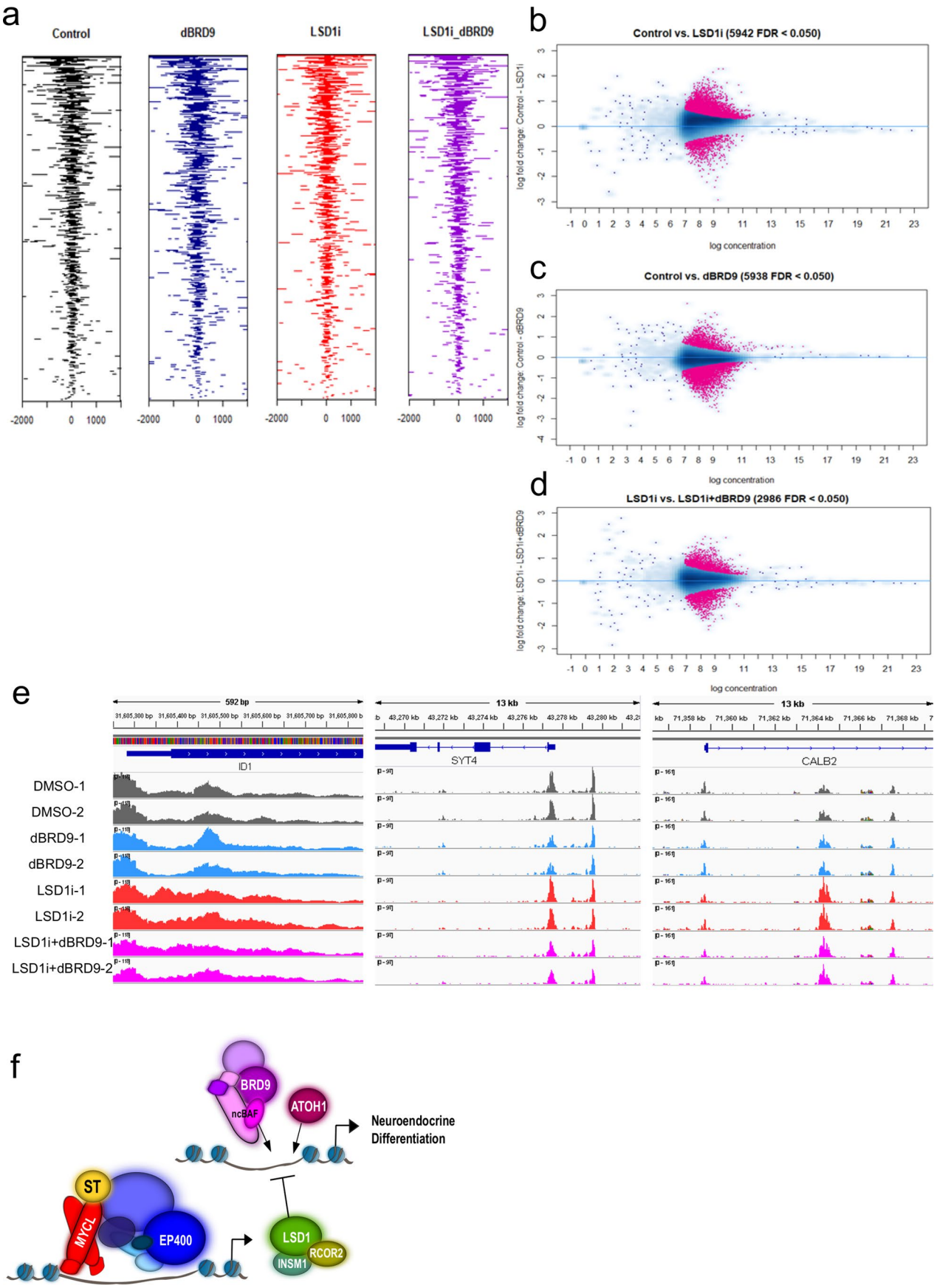

Extended Data Fig. 9 | See next page for caption.

Extended Data Fig. 9 | ATAC-seq of MKL-1 cells treated with LSD1 and BRD9 inhibitors suggests that BRD9 is required to de-repress a subset of LSD1 target genes. a, Tag heat maps of ATAC-seq peaks show open chromatin regions localize close to the transcription start sites (TSSs, +/- 2000 bp). Combined peaks from two replicates of ATAC-seq of MKL-1 cells treated with DMSO (Control), dBRD9 (0.1 μM), GSK-LSD1 (LSD1i, 0.1 μM), or both dBRD9 and LSD1i (LSD1i_dBRD9) are shown. **b**–**d**, The differentially enriched ATAC-seq peaks between Control vs. LSD1i (**b**), Control vs. dBRD9 (**c**), and LSD1i vs. LSD1i + dBRD9 (d) are shown with the peak abundance (log concentration) and log fold change in peak scores. The differentially enriched peaks were called using the Diffbind R package with the Wald test and FDR p-value correction. **e**, ATAC-seq peaks in the promoters of LSD1 target genes ID1, SYT4, and CALB2 with the mentioned conditions are shown. **f**, Model: Merkel cell polyomavirus activates LSD1-mediated blockade of non-canonical BAF to regulate transformation and tumorigenesis.

nature research

Corresponding author(s): James A. DeCaprio

Last updated by author(s): Mar 8, 2019

Reporting Summary

Nature Research wishes to improve the reproducibility of the work that we publish. This form provides structure for consistency and transparency in reporting. For further information on Nature Research policies, see Authors & Referees and the Editorial Policy Checklist.

Statistics

For all statistical analyses, confirm that the following items are present in the figure legend, table legend, main text, or Methods section.

n/a	Confirmed	
☐	☒	The exact sample size (*n*) for each experimental group/condition, given as a discrete number and unit of measurement
☐	☒	A statement on whether measurements were taken from distinct samples or whether the same sample was measured repeatedly
☐	☒	The statistical test(s) used AND whether they are one- or two-sided *Only common tests should be described solely by name; describe more complex techniques in the Methods section.*
☒	☐	A description of all covariates tested
☐	☒	A description of any assumptions or corrections, such as tests of normality and adjustment for multiple comparisons
☐	☒	A full description of the statistical parameters including central tendency (e.g. means) or other basic estimates (e.g. regression coefficient) AND variation (e.g. standard deviation) or associated estimates of uncertainty (e.g. confidence intervals)
☐	☒	For null hypothesis testing, the test statistic (e.g. *F*, *t*, *r*) with confidence intervals, effect sizes, degrees of freedom and *P* value noted *Give P values as exact values whenever suitable.*
☒	☐	For Bayesian analysis, information on the choice of priors and Markov chain Monte Carlo settings
☐	☒	For hierarchical and complex designs, identification of the appropriate level for tests and full reporting of outcomes
☒	☐	Estimates of effect sizes (e.g. Cohen's *d*, Pearson's *r*), indicating how they were calculated

Our web collection on statistics for biologists contains articles on many of the points above.

Software and code

Policy information about availability of computer code

Data collection	No software was used to collect data.
Data analysis	STAR 2.5.4a HTSeq 0.9.1 DESeq2 DAVID Bioinformatics Resources REVIGO Binding and Expression Target Analysis (BETA) BWA 0.7.13 MACS2 2.1.0 ChIPseeker 1.22.1 ChIPpeakAnno 3.20.0 DiffBind 2.14.0 Integrative genome viewer (IGV; Broad Institute) 2.8.x MAGeCK 0.5.9 MAGeCKFlute 1.6.3 GraphPad Prism DTASelect swalow QDNAseq Sequest ProLuCID Bowtie2 2.3.4 ReAdW.exe: Pedrioli, P.G., Eng, J.K., Hubley, R., Vogelzang, M., Deutsch, E.W., Raught, B., Pratt, B., Nilsson, E., Angeletti, R.H., Apweiler, R., et al. (2004). A common open representation of mass spectrometry data and its application to proteomics research. Nature

biotechnology 22, 1459-1466.

For manuscripts utilizing custom algorithms or software that are central to the research but not yet described in published literature, software must be made available to editors/reviewers. We strongly encourage code deposition in a community repository (e.g. GitHub). See the Nature Research guidelines for submitting code & software for further information.

Data

Policy information about availability of data

All manuscripts must include a data availability statement. This statement should provide the following information, where applicable:

- Accession codes, unique identifiers, or web links for publicly available datasets
- A list of figures that have associated raw data
- A description of any restrictions on data availability

https://www.ncbi.nlm.nih.gov/geo/query/acc.cgi?acc=GSE124864
http://proteomecentral.proteomexchange.org/cgi/GetDataset?ID=PXD012516

Field-specific reporting

Please select the one below that is the best fit for your research. If you are not sure, read the appropriate sections before making your selection.

☒ Life sciences ☐ Behavioural & social sciences ☐ Ecological, evolutionary & environmental sciences

For a reference copy of the document with all sections, see nature.com/documents/nr-reporting-summary-flat.pdf

Life sciences study design

All studies must disclose on these points even when the disclosure is negative.

Sample size	Sample size of 2-5 for molecular cell biology experiments (RT- and ChIP-qPCR, viability and soft agar colony assays) was determined by power calculation assuming an average effect fold change of 2.5 and standard deviation of 1.0.
Data exclusions	No data excluded
Replication	Biological experiments were performed independently to ensure reproducibility of the experimental outcomes. The manuscript only contains results that can be reproduced independently.
Randomization	Samples were randomly assigned into experimental groups.
Blinding	For the soft agar assay, the images were re-named by a colleague in the laboratory and the foci were counted in a blind manner.

Reporting for specific materials, systems and methods

We require information from authors about some types of materials, experimental systems and methods used in many studies. Here, indicate whether each material, system or method listed is relevant to your study. If you are not sure if a list item applies to your research, read the appropriate section before selecting a response.

Materials & experimental systems

n/a	Involved in the study
☐	☒ Antibodies
☐	☒ Eukaryotic cell lines
☒	☐ Palaeontology
☐	☒ Animals and other organisms
☒	☐ Human research participants
☒	☐ Clinical data

Methods

n/a	Involved in the study
☐	☒ ChIP-seq
☒	☐ Flow cytometry
☒	☐ MRI-based neuroimaging

Antibodies

Antibodies used

Rabbit polyclonal anti-LSD1 Cell Signaling Technology Cat# 2139; 1:3000
Mouse monoclonal anti-INSM1 (clone A-8) Santa Cruz Biotechnology Cat# sc-271408; 1:250
Rabbit polyclonal anti-RCOR2 Proteintech Group Cat# 23969-1-AP; 1:2000
Rabbit polyclonal anti-ID1 (C-20) Santa Cruz Biotechnology Cat# sc-488; 1:250
Rabbit polyclonal anti-MYCL1 Proteintech Group Cat# 14584-1-AP; 1:1000
Rabbit polyclonal anti-PROM1 (CD133) Proteintech Group Cat#18470-1-AP; 1:3000
Rabbit polyclonal anti-SMAD9 (aa-200-228) Lifespan Biosciences Cat# LS-C161303-400; 1:1000
Rabbit monoclonal anti-phospho-smad1(ser463/465)/smad5(ser463/465)/smad9(ser465/467) (clone D5B10) Cell signaling

technology Cat# 13820T; 1:3000
Rabbit polyclonal anti-ATOH1 Proteintech group Cat# 21215-a-AP; 1:2000
Rabbit polyclonal anti-SMARCA1 Cell signaling technology Cat# 9450S; 1:3000
Rabbit polyclonal anti-BRD9 Active motif Cat# 61537; 1:3000
Mouse monoclonal anti-BICRA (GLTSCR1) (clone H-10) Santa Cruz Biotechnology Cat# sc-515086; 1:250
Mouse monoclonal anti-BRG1(SMARCA4) (clone H-10) Santa Cruz Biotechnology Cat# sc-374197; 1:250
Rabbit monoclonal anti-Cleaved Notch1 (Val1744) Cell Signaling Technology Cat#; 1:3000
Rabbit monoclonal anti-HES1 (D6P2U) Cell Signaling Technology Cat#11988S; 1:3000
Rabbit polyclonal anti-H3 Cell Signaling Technology Cat#9715; 1:3000
Rabbit monoclonal anti-di-methyl-histone H3 (Lys4) (C64G9) Cell Signaling Technology Cat#9725; 1:3000
Rabbit polyclonal mono-methyl-histone H3 (Lys4) Active Motif Cat#61634; 1:2000
normal Rabbit IgG Cell signaling technology Cat#2729; 1:3000
Mouse monoclonal anti-MCV T antigens (clone AB5) Berrios, C. et al. Merkel Cell Polyomavirus Small T Antigen Promotes Pro-Glycolytic Metabolic Perturbations Required for Transformation. PLoS pathogens 12, doi:10.1371/journal.ppat.1006020 (2016).

Validation

Rabbit polyclonal anti-LSD1 : western blot (WB) and immunoprecipitation (IP) followed by mass spectrometry
Mouse monoclonal anti-INSM1 (clone A-8): WB and IP followed by mass spectrometry
Rabbit polyclonal anti-RCOR2: WB and IP followed by mass spectrometry
Rabbit polyclonal anti-ID1 (C-20): WB and IP followed by mass spectrometry
Rabbit polyclonal anti-MYCL1: WB, IP, immunohistochemistry (IHC), immunofluorescence (IF), (Flow cytometry (FC), CoIP, and ELISA
Rabbit polyclonal anti-PROM1 (CD133): WB, IHC, IF, FC, and ELISA
Rabbit polyclonal anti-SMAD9 (aa-200-228) : IF and WB
Rabbit monoclonal anti-phospho-smad1(ser463/465)/smad5(ser463/465)/smad9(ser465/467) (clone D5B10): WB, IP, IF and FC
Rabbit polyclonal anti-SMARCA1: WB and IP
Rabbit polyclonal anti-BRD9: ChIP-seq, IP, WB and IHC
Mouse monoclonal anti-BICRA (GLTSCR1) (clone H-10) :WB
Mouse monoclonal anti-BRG1(SMARCA4) (clone H-10) : WB, IP, and IF
Rabbit polyclonal anti-ATOH1: WB, IHC, IF, ELISA and IP followed by mass spectrometry
Mouse monoclonal anti-MCV T antigens (clone AB5): WB, IP followed by mass spectrometry, ChIP-seq, IF, and IHC
normal Rabbit IgG: IP and ChIP

Eukaryotic cell lines

Policy information about cell lines

Cell line source(s)

Human lung fibroblast: IMR90 ATCC Cat# CCL-186
Human MCC: MKL-1 (Shuda et al., 2008) Patrick S. Moore's laboratory at University of Pittsburgh
Human MCC: MKL-2 (Van Gele et al., 2002)Patrick S. Moore's laboratory at University of Pittsburgh
Human MCC: MS-1 (Shuda et al., 2008)Patrick S. Moore's laboratory at University of Pittsburgh
Human MCC: UISO (Ronan et al., 1993)Patrick S. Moore's laboratory at University of Pittsburgh
Human MCC: MCC13 (Leonard et al., 1995) Patrick S. Moore's laboratory at University of Pittsburgh
Human MCC: MCC26 (Leonard et al., 1995) Patrick S. Moore's laboratory at University of Pittsburgh
Human MCC: WaGa (Shuda et al., 2008) Jürgen Becker's laboratory at Medical University Graz, Austria
Human MCC: PeTa (Houben et al., 2013) Jürgen Becker's laboratory at Medical University Graz, Austria
Human MCC: BroLi (Shuda et al., 2008) Jürgen Becker's laboratory at Medical University Graz, Austria

Authentication

IMR90 were obtained directly from ATCC.
VP-MCC and VN-MCC lines were confirmed by sequencing (Oncopanel and various RNA-seq experiments). Oncopanel is targeted hybrid capture of 400 genes.

Mycoplasma contamination

All cell lines were negative for mycoplasma contamination.

Commonly misidentified lines
(See ICLAC register)

no commonly misidentified cell lines were used.

Animals and other organisms

Policy information about studies involving animals; ARRIVE guidelines recommended for reporting animal research

Laboratory animals	Mouse: NSG: NOD.Cg-Prkdcscid Il2rgtm1Wjl/SzJ The Jackson Laboratory Cat# 005557; Female; 4 to 6 weeks old.
Wild animals	the study did not involve wild animals.
Field-collected samples	the study did not involve samples collected from the field.
Ethics oversight	The animal studies were approved by the DFCI Institutional Animal Care and Use Committee (IACUC).

Note that full information on the approval of the study protocol must also be provided in the manuscript.

ChIP-seq

Data deposition

☒ Confirm that both raw and final processed data have been deposited in a public database such as GEO.

☒ Confirm that you have deposited or provided access to graph files (e.g. BED files) for the called peaks.

Data access links *May remain private before publication.*	https://www.ncbi.nlm.nih.gov/geo/query/acc.cgi?acc=GSE124864 Enter token ilqtmmycnfqvjsv into the box
Files in database submission	LSD1_1_sort_peaks.narrowPeak.bed LSD1_2_sort_peaks.narrowPeak.bed RCOR2_1_sort_peaks.narrowPeak.bed RCOR2_2_sort_peaks.narrowPeak.bed ATOH1_1_sort_peaks.narrowPeak.bed ATOH1_2_sort_peaks.narrowPeak.bed 20160525-LSD1-1-EP3066_S3_R1_001.fastq 20160525-LSD1-2-EP3066_S8_R1_001.fastq 20160525-RCOR2-1-EP3066_S4_R1_001.fastq 20160525-RCOR2-2-EP3066_S9_R1_001.fastq 20160525-ATOH1-1-EP3066_S5_R1_001.fastq 20160525-ATOH1-2-EP3066_S10_R1_001.fastq 20160525-Input-1-EP3066_S1_R1_001.fastq 20160525-Input-2-EP3066_S6_R1_001.fastq
Genome browser session (e.g. UCSC)	https://genome.ucsc.edu/s/donglim618/Park_LSD1_RCOR2_ATOH1_ChIPseq

Methodology

Replicates	There are two biologically and technically independent ChIP replicates. Data for each replicate (not combined) are shown in figures.
Sequencing depth	LSD1_1: tag size is determined as 75 bps total tags in treatment: 39138041 tags after filtering in treatment: 36570635 maximum duplicate tags at the same position in treatment = 1 Redundant rate in treatment: 0.07 total tags in control: 41807511 tags after filtering in control: 38806784 maximum duplicate tags at the same position in control = 1 Redundant rate in control: 0.07 d = 146 LSD1_2: tag size is determined as 75 bps total tags in treatment: 49000665 tags after filtering in treatment: 45049086 maximum duplicate tags at the same position in treatment = 1 Redundant rate in treatment: 0.08 total tags in control: 42349718 tags after filtering in control: 39249637 maximum duplicate tags at the same position in control = 1 Redundant rate in control: 0.07 d = 146 RCOR2_1:

tag size is determined as 75 bps
total tags in treatment: 46679427
tags after filtering in treatment: 42544637
maximum duplicate tags at the same position in treatment = 1
Redundant rate in treatment: 0.09
total tags in control: 41807511
tags after filtering in control: 38806784
maximum duplicate tags at the same position in control = 1
Redundant rate in control: 0.07
d = 146

RCOR2_2:
tag size is determined as 75 bps
total tags in treatment: 47063218
tags after filtering in treatment: 43247674
maximum duplicate tags at the same position in treatment = 1
Redundant rate in treatment: 0.08
total tags in control: 42349718
tags after filtering in control: 39249637
maximum duplicate tags at the same position in control = 1
Redundant rate in control: 0.07
d = 146

ATOH1_1:
tag size is determined as 75 bps
total tags in treatment: 48801832
tags after filtering in treatment: 42904152
maximum duplicate tags at the same position in treatment = 1
Redundant rate in treatment: 0.12
total tags in control: 41807511
tags after filtering in control: 38806784
maximum duplicate tags at the same position in control = 1
Redundant rate in control: 0.07
d = 146

ATOH1_2:
tag size is determined as 75 bps
total tags in treatment: 50778490
tags after filtering in treatment: 45829530
maximum duplicate tags at the same position in treatment = 1
Redundant rate in treatment: 0.10
total tags in control: 42349718
tags after filtering in control: 39249637
maximum duplicate tags at the same position in control = 1
Redundant rate in control: 0.07
d = 146

Antibodies

Rabbit polyclonal anti-LSD1 Cell Signaling Technology Cat# 2139
Rabbit polyclonal anti-RCOR2 Proteintech Group Cat# 23969-1-AP
Rabbit polyclonal anti-ATOH1 Proteintech group Cat# 21215-a-AP

Peak calling parameters

Peaks were called using using the default parameters (band width = 300, model fold = [5, 50], qvalue cutoff = 1.00e-02 and tag size is determined as 75 bps)of MACS2 v2.1.0 relative to the input samples. .narrwPeak.bed files were generated using MACS2 v2.1.0.

Data quality

With the qvalue cutoff = 1.00e-02,
LSD1_1: 68197 peaks
LSD1_2: 30688 peaks
RCOR2_1: 62798 peaks
RCOR2_2: 33899 peaks
ATOH1_1: 106317 peaks
ATOH1_2: 86123 peaks

Software

ChIPseeker
ChIPpeakAnno
DiffBind
Integrative genome viewer (IGV; Broad Institute)